THE ASTRONOMICAL JOURNAL VOLUME 99, NUMBER 2 FEBRUARY 1990

A MULTICOLOR PHOTOMETRIC STUDY OF THE TIDAL FEATURES IN INTERACTING GALAXIES

JAMES M. SCHOMBERT
Department of Astronomy, University of Michigan, Ann Arbor, Michigan 48109

JOHN F. WALLIN AND CURTIS STRUCK-MARCELL
Astronomy Program, Department of Physics, Iowa State University, Ames, Iowa 50011
Received 14 August 1989; revised 2 November 1989

ABSTRACT

Four-color surface photometry (*BVri*) is presented for low-surface-brightness tidal features in interacting galaxies. Objects were selected on the basis of visual morphology including a cross section of tails, bridges, plumes, shells, and extended envelopes. Intensity cross sections and surface brightness suggests that plumes are face-on or near face-on sheets; tails and bridges are more nearly one-dimensional, linear figures. In many cases the colors of tidal features are similar to the outer regions of the primary galaxies, confirming the stripping origin hypothesis. However, large color variations are found among the morphological components within most systems, and within individual components. Blue colors in primaries and tidal features are most dramatic in $B - V$, not $V - i$ indicating that star formation, not metallicity or age, is the dominant component. There is clear evidence in our sample of a correlation between the magnitude of the color variation and the time since the beginning of the interaction as determined by the development of the tidal features. The color variations are largest a short time after the beginning of the interaction, and they diminish to a very low level in merged systems. This correlation provides an alternate estimator of interaction age in systems with ambiguous morphologies, and another constraint to aid in understanding the nature of star formation in interacting systems. On average, 25% of a system's luminosity is tied to tidal features for, although low in surface brightness, their projected area is large.

I. INTRODUCTION

The nonlinear disturbances and extended morphologies of interacting galaxies provide a dramatic view of the processes that drive galaxy evolution. A rapidly growing literature of numerical experiments documents our steadily increasing understanding of the stellar and gas dynamical processes that produce the peculiar morphologies in interacting galaxies (e.g., Toomre and Toomre 1972, hereafter referred to as TT; Noguchi and Ishibashi 1986; Noguchi 1987; Barnes 1988; Hernquist and Quinn 1989). This work gives us some idea of (1) the duration of transient tidal features such as bridges, tails, and plumes, (2) at what stage of an interaction such features are produced, and (3) what type of precursor galaxies and orbital parameters are required to produce particular features, and (4) what are the long-term consequences (e.g., merger, bar formation, etc.) of an interaction.

Our understanding of the relations between interactions and enhanced star formation is much less well-developed than our understanding of peculiar morphology. The observational studies carried out to date show that these relations may be quite complex. Historically, the blue photos in the atlases of Arp (1966) and Vorontsov-Velyaminov (1959) gave early evidence that very blue colors are not uncommon among interacting galaxies. Larson and Tinsley (1978, hereafter referred to as LT) carried out the first systematic study of the colors of interacting galaxies, and found that even more than blueness, the Arp atlas galaxies were characterized by large color variations (from system to system). LT also found that they could account for most of these variations as the result of a single recent burst of star formation, superimposed on an older stellar population. The color variations in their evolutionary models depended on one free parameter—the burst strength—as well as time, i.e., the aging of the burst. Reddening could account for some of the galaxies with colors which did not fit within the model grid. LT's seminal result (together with the work of Huchra 1977; Struck-Marcell and Tinsley 1978; Rieke *et al.* 1980) posed many questions. For example, when do starbursts occur in interacting galaxies and what determines their strength? These questions, and the general focus on bursts, have dominated the study of star formation in interacting galaxies up to the present.

In the time since LT's paper a number of methods besides broadband colors have been used to gauge star formation in interacting galaxies (see Kennicutt 1989 for a review of these methods). Early near-infrared photometry showed that starbursts occur in a region within a few kiloparsecs of the nucleus in a number of nearby systems (see, e.g., the review of Telesco 1984). *IRAS* data combined with near-infrared photometry confirm the importance of nuclear starbursts in interacting systems (e.g., Joseph and Wright 1985; Telesco, Wolstencroft, and Done 1988; Soifer *et al.* 1987). *IRAS* data have also revealed the super-starburst phenomena in apparent merger remnants.

Meanwhile, Hα studies (Keel *et al.* 1985; Bushouse 1986; Kennicutt *et al.* 1987) have confirmed a number of LT's original results, including: (1) that star formation is, on average, enhanced in interacting galaxies, (2) that system-to-system variations are large, and (3) that in a certain fraction of interacting galaxies, star formation is not noticeably enhanced. Moreover, Bushouse's (1986) study of "violent" interactions and Kennicutt *et al.* (1987) comparison of a sample of close pairs to a more strongly interacting sample of Arp galaxies, have lead to the conclusion that the degree of star-formation enhancement correlates with the vigor of the interaction. Combined with radio-continuum observations (e.g., Condon 1983) these optical and infrared observations leave little doubt that interactions enhance star formation. The Hα observations also show that this star formation can

 0004-6256/90/020497-33$00.90

be very extended. However, the evident explanation is the increased reddening in the central regions. Thus, both central and extended enhancements occur, though not necessarily at the same time or in all systems.

The Hα observations also give some indication that enhanced star formation occurs in very extended tidal features, although little of this data has been published yet. The main purpose of the present study is to determine the color characteristics of the generally low-surface-brightness tidal features, using CCD photometry. In addition to allowing the study of these extended features, the multicolor photometry also enables us to study color variations down to quite small scales within the interacting systems.

As always, such color variations are likely to be the product of two processes—enhanced star formation and differential reddening. The importance of differential reddening is obvious just from the fact that the colors of otherwise identical disks will depend on inclination (some apparent examples are discussed below). On the other hand, the role of reddening in the dynamically evolving tidal features is a largely unexplored area at present. Nonetheless, while the uncertainties connected with reddening will be a recurring theme in this paper, we do not believe they prevent us from obtaining useful information about star formation in the tidal features.

Such information is important not only for determining whether or not star formation is enhanced in the outermost regions of interacting galaxies, but also for constraining the mechanisms, and determining when such star formation occurs. The large spatial scales of tidal features are the chief advantage in studying mechanisms, especially wave-induced star formation. The fact that dynamical models can reveal the sequence through which various tidal morphologies appear and provide the relative timescales for their development, means that tidal morphologies can be used to measure the time since the onset of the disturbance (e.g., TT). This morphology clock generally measures longer intervals (dynamical timescales) than OB star lifetimes or gas consumption timescales in starburst nuclei. Thus, by comparing the distribution of colors in systems with different "morphological ages," we can hope to make a provisional assessment of when and where enhanced star formation occurs. This would allow a refinement of LT's hypothesis that such star formation can be accounted for by a single burst, revealing for example, whether it is a sequence of bursts, or bursts propagating in waves across the system (see Struck-Marcell and Appleton 1987).

The data used in this work consist of CCD frames in four colors collected during the 1985 to 1987 observing seasons. In Sec. II, the data and reduction procedures are described. In Sec. III, the analysis technique is developed, individual objects are discussed, and the limitations from errors are presented. In Sec. IV, the general color and structure trends are outlined and comparisons are made to models of the star formation and interaction dynamics.

II. OBSERVATIONS

The sample for this study was selected from the Arp Atlas (Arp 1966) with the primary criteria based on optical morphology indicative of a tidal interaction. This selection was guided by comparison to simulations of collisions in the literature (TT) and typical structures detected in interacting systems as deduced by dynamical studies (Schweizer 1986). The sample was imaged on the Palomar 1.5 m telescope. The photon collector was a RCA CCD of 320×512 pixels. This device has $30e^-$ readout noise and a conversion factor of $6e^-$/DN. Reimaging optics were used to expand the field size to 6.6×10.5 arcmin. This enabled photometry of large extended plumes and tails and increased the number of counts per pixel to well above the readout noise, but resulted in large pixels (1.23 arcsec). However, the data were in any case rebinned to 5 arcsec pixels to increase the signal-to-noise of low-surface-brightness features (see Sec. III).

For various historical reasons, the filter system at the 1.5 m telescope consists of pseudo-Johnson *B*, Johnson *V*, Gunn *r*, and Gunn *i*, instead of a pure Johnson–Cousins or Kron–Cousins system. This filter set has effective wavelengths of 4200, 5400, 6500, and 8200 Å. The *B* filter is unusual in that it is slightly narrower than a normal Johnson *B* (700 Å FWHM versus the standard 1000 Å). Consequently, using the Palomar 1.5 m *B* filter results in fewer counts per second; however, the color term in the photometric constants is reduced relative to a standard Johnson *B* filter. The FWHM of the *V*, *r*, and *i* filters are 1000, 1000, and 1500 Å, respectfully. This is an awkward setup for any observing program since two separate sequences of standards must be taken each night to calibrate the blue Johnson filters and the red Gunn filters. It is also difficult to properly define the Gunn filters, since many of the standards from Kent (1985) are too bright ($m_V < 10$) for the 1.5 m and saturate the chip in the minimum allowed 1 s exposure time. The standards must, therefore, be taken out of focus, leading to scattered light and overlapping image problems. Another problem for the Gunn system is the very small number of blue standards ($B - V < 0.5$, particularly in the fall sky) which are critical for any project dealing with star-forming galaxies.

In order to eliminate the problems outlined above, a program was undertaken during the 1986–1987 observing season to transform Landolt (1983) standards onto the Gunn system. A good range of color was selected to develop the zero points and color terms; however, the zero points quoted below are based on the stars HD 19445, HD 140283, and Ross 484 (Bessell, private communication). The derived transformations from Cousins to Gunn filters (Barsony 1988) are:

$$r = R_c + 0.280 + 0.038(R_c - I_c),$$
$$i = I_c + 0.605 + 0.067(R_c - I_c).$$

The reader is cautioned that these transformations are only first-order approximations sufficient for the data in this study and tailored to the Palomar CCD system and extinction coefficients.

The software package ARCHANGEL was used for reduction of the raw CCD data. The first step was erase level subtraction, the erase level being determined from 50 lines of overscan taken after each frame was read out. For exposures longer than 5 min, it was also necessary to subtract a dark frame of equal duration to remove noise from a hot amplifier on the south side of the CCD. These dark frames were collected during the daylight hours, and consisted of averages of 10 frames for each exposure time. Flatfields were obtained from dome illuminated short exposures taken at least five times during the night, and flattening was good to the 0.3% level in the red, 0.1% in the blue. Masks were applied to flattened data to flag one bad column and two regions of depressed chip sensitivity. Regions for sky determination were located interactively on a graphics display. These regions usually consisted of 8–10 boxes of 20×20 pixels locat-

ed in a symmetrical pattern around the objects of interest; but, avoiding low-surface-brightness features, halos of bright stars or any other objects that might degrade the sky estimate. Extinction corrected sky magnitudes and the sky error are presented in Table I along with a log of the observations.

For accurate pixel by pixel, or grid, photometry (also called two-color mapping, see Bothun 1986), a critical step is to register each frame to a common origin so that the pixel by pixel comparison is not distorted. In this case, all stellar images above a 2.5σ threshold of sky are located and analyzed for their centroids. Double stars and galaxies could be eliminated from their second moments. Each set of images is compared to the *B* frame set of images and the corresponding transformations are calculated. Rotation and expansion terms were always negligible, so that only corrections to linear coordinates were required. After transformation, the set of images from the *r* frame was used to produce a mask to eliminate all objects not related to the interacting system. Last, the masked frames were displayed and cleaned of cosmic rays with an interactive median filter (i.e., a mobile box of 10×10 pixels). For grid photometry, the data in each frame were then rebinned into 4 arcsec pixels to increase the signal-to-noise and subtracted to produce an instrumental color frame. This frame could then be interrogated or used to produce a spatial plot.

III. ANALYSIS

a) Methods

The end product from the reduction of the raw data can be divided into three categories; luminosities, colors, and structure. The luminosities quoted herein are isophotal visual magnitudes determined from cleaned *V* frames. The procedure was to outline a irregular polygon shape around the object of interest (either a primary galaxy or a tidal feature) and to sum all the counts above a specified threshold. A threshold level of 26.0 *V* mag arcsec^{-2} was used for all the luminosities quoted. Every possible effort was made to select boundaries so that the derived luminosities of tidal features were not contaminated by galaxy light and vice versa. Stars and other non-extragalactic features were deleted from the data before reduction, but none of these regions contained a significant fraction of any object's light. Average and peak surface brightnesses are also determined within the areas selected.

Colors were calculated in a slightly different fashion. The procedure for colors was to take the cleaned frames and sum 4×4 pixel boxes (24 sq. arcsec). These summed files were than subtracted and converted to instrumental colors. Total colors could then be determined by averaging, with a maximum-likelihood method, all the boxes within the same polygons used for the luminosity calculation above. This procedure allows an increase in the signal-to-noise for faint features, while preserving some of the geometrical information with respect to color. It also allows an error estimate for color based on the dispersion for the many individual measures within the tidal feature itself. The averaged colors are weighted by surface brightness of each box. Unfortunately, this can lead to misleading values, particularly for objects with strong color gradients such as a red, high-surface-brightness bulges versus blue, low-surface-brightness disks (e.g., object A of Arp 102). However, inspection of the color histograms and the spatial color maps resolves any ambiguity. Luminosities, surface brightnesses, and colors are listed in Table II for the primary galaxies and tidal features in the sample. The reader is referred to the discussion of the individual objects below for further information on the identity of each feature. Note that the error values quoted in Table II are dispersions from the mean value. The true error was dependent on surface brightness; however, in only a few faint features was the instrumental error greater than the true range of color within the features.

Grid photometry is the adopted procedure for inspection of the spatial extent of color variations in nonsymmetric objects such as tidal features. The simplest method is to represent the two-dimensional image of the galaxy with a lookup table that corresponds to color rather than luminosity. However, these plots are also deceptive in overemphasizing radial gradients or coherent color structure rather than real variations in color on small scales. To this end, this paper has elected display color structure as a series of slices through the two-dimensional image where each box within the color range is represented by a single dot. Proper selection of the spacing and range of color should reveal the correct magnitude in variations plus provide a direct comparison with other systems. The actual procedure was to apply a surface-brightness threshold of 26 *B* mag arcsec^2 to the galaxies and features in the *B* frame so that each box above this threshold is marked and its value in all four filters is extracted for use in the two-color plots (Figs. 1–8). This is the best approach since (a) the *B* CCD frames were the weakest in individual pixel S/N, (b) the sky brightness is the darkest in this frame (maximal astrophysical cause to the detection rather than sky noise), and (c) image quality was usually best in the *B* frames (although this is not as important for the 5×5 arcsec boxes used). There is a natural bias in our system towards red detections since CCD response peaks in the *V* and *r* filters. Thus, we have offset this bias with an effort to hinge detections on higher blue surface-brightness regions, regions of star formation. The immediate consequence of this threshold criteria is an artificially low calculation of the internal error on a pixel$\times$pixel basis. Calculations of this style, often applied in photometry, do not take into account the errors between frames such as guiding errors, poor frame registration, or color terms, although every effort was made during software development to minimize these problems. A series of robustness tests were made during software development and their results, as applied to the dataset herein, can be summarized by the statement "if bright blue and red regions are detected in low-surface-brightness features they do exist." Variations in color greater than 0.4 mag are detectable with the thresholds applied here. However, pixel$\times$pixel colors near threshold will be dominated by random noise and weighted averages are superior for actual color determination.

Last, structural parameters (i.e., scale lengths and mean surface brightness) were determined in two fashions. The first is through the use of simple cuts across the shortest and longest lengths of the tidal features converted to surface brightness in mag arcsec^{-2}. The second procedure is contour fitting of ellipses to the primary objects. This later procedure is used exclusively to determine the luminosity, colors, and structure of extended envelopes (e.g., Arp 169 and Arp 170) since their radial symmetry precludes isolating the envelope from the primary galaxies in the same fashion as was used for linear features such as tails. The descriptive terms for the particular structural features (e.g., tails, plumes, etc.) are discussed in the next section.

TABLE I. Observations.

Object	File	E	k	Filter	Sky Mag.	Sky Error
Arp 96	P1186.259	1200	1.67	B	22.19	0.34%
	P1186.258	600	1.67	V	20.82	0.30%
	P1186.260	600	1.67	r	20.78	0.18%
	P1186.261	600	1.67	i	19.42	0.34%
Arp 97	P0187.273	900	1.05	B	22.57	0.32%
	P0187.274	600	1.07	V	21.42	0.18%
	P0187.272	600	1.03	r	21.26	0.25%
	P0187.271	600	1.02	i	20.23	0.20%
Arp 100	P1186.117	1200	1.45	B	21.87	0.26%
	P1186.116	600	1.43	V	20.52	0.18%
	P1186.118	600	1.50	r	20.36	0.18%
	P1186.119	600	1.52	i	19.12	0.33%
Arp 101	P0686.221	600	1.08	B	22.69	0.53%
	P0686.220	300	1.08	V	21.69	0.60%
	P0686.222	300	1.07	r	21.47	0.48%
	P0686.223	300	1.06	i	20.14	0.64%
Arp 102	P0686.247	600	1.09	B	22.68	0.53%
	P0686.246	300	1.08	V	21.67	0.30%
	P0686.248	300	1.10	r	21.61	0.16%
	P0686.249	300	1.11	i	20.15	0.46%
Arp 103	P0686.356	600	1.08	B	22.82	0.48%
	P0686.355	300	1.07	V	21.76	0.23%
	P0686.357	300	1.10	r	21.62	0.20%
	P0686.358	300	1.11	i	20.08	0.27%
Arp 104	P0686.217	600	1.17	B	22.70	0.75%
	P0686.216	300	1.16	V	21.70	0.36%
	P0686.218	300	1.18	r	21.46	0.21%
	P0686.219	300	1.18	i	20.03	0.33%
Arp 105	P0187.355	900	1.01	B	22.54	0.46%
	P0187.354	600	1.00	V	21.39	0.21%
	P0187.356	600	1.01	r	21.17	0.14%
	P0187.357	600	1.02	i	19.98	0.23%
Arp 169	P0686.361	600	1.33	B	22.56	0.44%
	P0686.362	300	1.27	V	21.61	0.36%
	P0686.363	300	1.20	r	21.45	0.50%
	P0686.364	300	1.19	i	20.11	0.48%
Arp 170	P1186.309	1200	1.03	B	22.35	0.77%
	P1186.308	600	1.03	V	21.11	0.19%
	P1186.310	600	1.04	r	20.92	0.08%
	P1186.311	600	1.05	i	19.77	0.28%
Arp 172	P0686.347	600	1.12	B	22.67	0.52%
	P0686.348	300	1.14	V	21.63	0.36%
	P0686.346	300	1.11	r	21.45	0.50%
	P0686.345	300	1.10	i	20.04	0.23%
Arp 173	P0686.324	600	1.09	B	22.50	1.21%
	P0686.323	300	1.09	V	21.49	0.21%
	P0686.325	300	1.10	r	21.34	0.25%
	P0686.326	300	1.10	i	20.04	0.10%
Arp 179	P1186.131	1200	1.32	B	22.07	0.43%
	P1186.130	600	1.30	V	20.71	0.22%
	P1186.132	600	1.35	r	20.50	0.26%
	P1186.133	600	1.38	i	19.11	0.38%
Arp 190	P1186.245	1200	1.09	B	22.12	0.25%
	P1186.244	600	1.08	V	20.95	0.15%
	P1186.246	600	1.12	r	20.86	0.15%
	P1186.247	600	1.14	i	19.64	0.23%
Arp 193	P0686.316	600	1.01	B	22.56	0.56%
	P0686.315	300	1.01	V	21.54	0.11%
	P0686.317	300	1.01	r	21.38	0.10%
	P0686.318	300	1.01	i	20.01	0.27%
Arp 204	P0686.321	600	1.60	B	22.30	0.44%
	P0686.322	300	1.60	V	21.23	0.28%
	P0686.320	300	1.60	r	21.07	0.36%
	P0686.319	300	1.60	i	19.71	0.22%
Arp 222	P1186.113	1200	1.43	B	21.86	0.81%
	P1186.112	600	1.43	V	20.57	0.33%
	P1186.114	600	1.44	r	20.37	0.60%
	P1186.115	600	1.45	i	19.18	0.25%
Arp 223	P1186.209	1200	1.27	B	21.95	0.70%
	P1186.208	600	1.27	V	20.74	0.31%
	P1186.210	600	1.27	r	20.56	0.30%
	P1186.211	600	1.28	i	19.38	0.23%
Arp 232	P0187.249	900	1.10	B	22.29	0.51%
	P0187.250	300	1.12	V	21.13	0.33%
	P0187.248	300	1.10	r	20.99	0.44%
	P0187.247	300	1.09	i	19.10	0.27%
Arp 242	P0686.213	300	1.04	B	22.54	0.55%
	P0686.212	300	1.04	V	21.54	0.14%
	P0686.214	300	1.05	r	21.43	0.26%
	P0686.215	300	1.05	i	20.12	0.18%
Arp 243	P1186.154	1200	1.01	B	21.82	0.26%
	P1186.153	600	1.02	V	20.78	0.04%
	P1186.155	600	1.01	r	20.71	0.14%
	P1186.156	600	1.01	i	19.50	0.27%
Arp 245	P0187.339	1200	1.76	B	22.22	0.42%
	P0187.337	600	1.83	V	21.01	0.13%
	P0187.340	600	1.74	r	21.08	0.31%
	P0187.341	600	1.72	i	19.96	0.48%
Arp 252	P0187.344	1200	1.71	B	22.22	0.70%
	P0187.345	600	1.68	V	20.99	0.13%
	P0187.343	600	1.74	r	20.98	0.10%
	P0187.342	600	1.77	i	19.85	0.28%
Arp 295	P1186.409	1200	1.25	B	22.06	0.41%
	P1186.408	600	1.26	V	20.92	0.23%
	P1186.410	600	1.25	r	20.74	0.28%
	P1186.411	600	1.26	i	19.65	0.26%
Arp 319	P0686.254	600	1.16	B	22.31	0.80%
	P0686.253	300	1.18	V	21.40	0.48%
	P0686.255	300	1.14	r	21.34	0.57%
	P0686.256	300	1.13	i	20.05	0.40%

TABLE II. Primary galaxy and tidal feature data.

Object	Feature	Type	V_{26}	$\bar{\mu}$	μ_c	$B-V$	$V-r$	$r-i$
Arp 96 [S+E]	A	galaxy	14.75	22.46	19.79	1.05 ±0.07	0.27 ±0.07	0.44 ±0.12
	B	galaxy	14.03	22.12	19.04	1.05 ±0.06	0.26 ±0.06	0.46 ±0.09
	C	plume	16.37	24.60	23.19	1.32 ±0.32	0.43 ±0.12	0.85 ±0.26
	D	bridge	15.93	24.11	23.07	1.18 ±0.18	0.40 ±0.08	0.75 ±0.14
Arp 97 [E+S]	A	galaxy	14.97	22.28	18.95	0.85 ±0.09	0.13 ±0.04	0.19 ±0.14
	B	galaxy	15.16	22.28	19.29	0.49 ±0.11	0.06 ±0.07	0.11 ±0.10
	C	bridge	16.09	23.99	22.89	0.62 ±0.16	0.09 ±0.08	0.16 ±0.11
	D	plume	16.00	23.68	21.78	0.39 ±0.13	-0.04 ±0.10	0.08 ±0.11
Arp 100 [S+E]	A	galaxy	14.80	22.79	20.36	0.84 ±0.13	0.19 ±0.08	0.32 ±0.15
	B	galaxy	14.09	21.92	19.10	0.83 ±0.13	0.14 ±0.08	0.48 ±0.41
	C	tail	16.15	24.45	23.28	0.48 ±0.26	0.04 ±0.13	0.30 ±0.28
	D	plume	16.45	24.79	23.61	0.57 ±0.27	-0.16 ±0.22	0.31 ±0.41
Arp 101 [S+E]	A	galaxy	14.36	22.10	19.40	0.81 ±0.09	0.20 ±0.07	0.69 ±0.34
	B	galaxy	14.48	22.41	19.53	0.86 ±0.06	0.20 ±0.03	0.69 ±0.30
	C	tail	15.93	24.60	23.28	0.61 ±0.34	0.15 ±0.13	0.54 ±0.26
	D	plume	15.62	24.41	23.20	0.79 ±0.25	0.19 ±0.09	0.66 ±0.21
Arp 102 [S+E]	A	galaxy	13.85	22.38	19.17	0.72 ±0.19	0.16 ±0.10	0.51 ±0.27
	B	galaxy	14.36	22.12	18.54	0.88 ±0.09	0.18 ±0.09	0.57 ±0.29
	C	tail	15.00	24.29	22.81	0.51 ±0.18	0.09 ±0.10	0.61 ±0.18
	D	bridge	16.98	25.06	23.93	0.46 ±0.52	0.18 ±0.17	0.81 ±0.39

TABLE II. (continued)

Object	Feature	Type	V_{26}	$\bar{\mu}$	μ_c	$B-V$	$V-r$	$r-i$
Arp 103 [S+E]	A	galaxy	15.06	22.26	19.13	0.78 ±0.06	0.12 ±0.05	0.51 ±0.12
	B	galaxy	14.22	21.98	18.40	0.90 ±0.08	0.18 ±0.04	0.57 ±0.18
	C	bridge	17.20	24.81	23.73	0.48 ±0.51	0.13 ±0.14	0.62 ±0.18
	D	galaxy	15.73	22.46	19.65	0.79 ±0.07	0.13 ±0.04	0.52 ±0.25
Arp 104 [S+E]	A	galaxy	12.44	21.99	19.56	0.63 ±0.12	0.11 ±0.07	0.51 ±0.14
	B	galaxy	13.25	21.81	18.69	0.79 ±0.06	0.16 ±0.03	0.60 ±0.13
	C	plume	16.09	24.93	23.48	0.31 ±0.51	0.00 ±0.19	0.51 ±0.31
	D	bridge	15.49	24.75	23.72	0.56 ±0.31	0.10 ±0.14	0.60 ±0.25
	E	tail	15.40	23.66	22.35	0.60 ±0.16	0.11 ±0.06	0.55 ±0.12
Arp 105 [S+E]	A	galaxy	14.55	22.76	19.68	0.72 ±0.11	0.09 ±0.08	0.21 ±0.15
	B	galaxy	13.95	22.35	19.16	0.92 ±0.09	0.13 ±0.04	0.25 ±0.11
	C	disk(?)	15.81	24.36	22.80	0.37 ±0.15	-0.05 ±0.09	0.22 ±0.18
	D	bridge	16.47	24.89	23.41	0.54 ±0.32	0.03 ±0.13	0.37 ±0.28
Arp 169 [E+E]	A	galaxy	14.00	21.23	18.39	0.97 ±0.04	0.18 ±0.04	0.59 ±0.07
	B	galaxy	14.50	21.22	19.24	1.01 ±0.03	0.22 ±0.04	0.62 ±0.06
	C	envelope	14.18	23.46	22.36	0.99 ±0.10	0.21 ±0.04	0.65 ±0.10
Arp 170 [E+E]	A	galaxy	14.35	21.22	18.98	1.05 ±0.08	0.21 ±0.02	0.39 ±0.07
	B	galaxy	14.81	21.35	19.01	1.08 ±0.03	0.22 ±0.02	0.37 ±0.07
	C	envelope	14.23	23.27	22.06	1.04 ±0.16	0.22 ±0.04	0.41 ±0.06

TABLE II. (continued)

Object	Feature	Type	V_{26}	$\bar{\mu}$	μ_c	$B-V$	$V-r$	$r-i$
Arp 172 [E+E]	A	galaxy	14.32	21.53	18.33	0.95 ±0.06	0.22 ±0.02	0.56 ±0.12
	B	galaxy	15.17	22.16	19.24	1.03 ±0.07	0.23 ±0.05	0.58 ±0.17
	C	plume	15.51	24.01	22.92	1.00 ±0.19	0.22 ±0.05	0.63 ±0.09
	D	plume	15.85	24.12	22.96	1.02 ±0.17	0.21 ±0.06	0.60 ±0.12
Arp 173 [S+S]	A	galaxy	14.28	22.12	18.64	0.66 ±0.07	0.13 ±0.07	0.44 ±0.19
	B	galaxy	15.51	22.45	19.25	0.62 ±0.07	0.18 ±0.07	0.43 ±0.25
	C	tail	17.06	24.54	23.16	0.71 ±0.29	0.09 ±0.11	0.58 ±0.21
Arp 179 [merger?]	A	galaxy	15.39	22.90	19.65	0.72 ±0.08	0.18 ±0.06	0.18 ±0.23
	B	tail	16.82	24.41	23.19	0.56 ±0.20	0.08 ±0.10	0.28 ±0.24
Arp 190 [triple]	A	galaxy	15.84	22.98	21.25	0.55 ±0.10	0.06 ±0.06	0.13 ±0.13
	B	galaxy	15.15	22.49	20.11	0.91 ±0.16	0.21 ±0.07	0.33 ±0.10
	C	galaxy	14.38	22.52	19.09	1.04 ±0.06	0.21 ±0.03	0.37 ±0.11
	D	tail	16.66	24.42	23.34	0.73 ±0.26	0.17 ±0.08	0.18 ±0.20
	E	bridge	18.08	25.14	24.54	0.92 ±0.56	0.28 ±0.17	0.58 ±0.35
Arp 193 [merger]	A	galaxy	14.24	21.86	19.75	0.40 ±0.09	0.07 ±0.08	0.37 ±0.19
	B	tail	16.43	23.84	22.58	0.44 ±0.15	0.07 ±0.06	0.41 ±0.14
	C	tail	16.58	24.30	23.23	0.38 ±0.15	0.00 ±0.07	0.41 ±0.21
Arp 204 [S+S]	A	galaxy	15.26	22.47	20.12	0.43 ±0.07	0.08 ±0.08	0.31 ±0.13
	B	galaxy	15.76	22.47	20.49	0.65 ±0.17	0.24 ±0.08	0.52 ±0.16
	C	tail	17.04	23.51	21.70	0.25 ±0.08	0.04 ±0.08	0.18 ±0.18
	D	bridge	17.03	24.09	22.62	0.43 ±0.14	0.07 ±0.08	0.40 ±0.12

TABLE II. (continued)

Object	Feature	Type	V_{26}	$\bar{\mu}$	μ_c	$B-V$	$V-r$	$r-i$
Arp 222 [merger]	A	center	12.10	19.81	19.09	0.75 ±0.16	0.15 ±0.02	0.39 ±0.14
	B	envelope	12.24	23.93	22.19	0.90 ±0.19	0.12 ±0.09	0.40 ±0.20
Arp 223 [merger]	A	center	12.56	20.13	19.05	0.96 ±0.06	0.20 ±0.01	0.82 ±0.11
	B	envelope	12.11	23.12	20.86	0.93 ±0.05	0.21 ±0.04	0.75 ±0.08
Arp 232 [merger]	A	center	13.09	20.26	18.22	1.00 ±0.11	0.19 ±0.05	1.06 ±0.07
	B	envelope	12.26	22.98	21.08	0.91 ±0.08	0.22 ±0.05	1.08 ±0.07
Arp 242 [S+S]	A	galaxy	14.36	21.79	20.59	0.75 ±0.09	0.17 ±0.06	0.60 ±0.14
	B	galaxy	14.08	21.47	19.66	0.75 ±0.12	0.17 ±0.06	0.58 ±0.16
	C	tail	15.11	23.38	21.95	0.59 ±0.14	0.10 ±0.04	0.42 ±0.17
	D	plume	15.60	24.45	23.24	0.53 ±0.37	0.13 ±0.10	0.65 ±0.15
Arp 243 [merger]	A	galaxy	13.81	21.75	19.20	0.47 ±0.13	0.02 ±0.07	0.20 ±0.13
	B	tail	15.81	23.76	21.70	0.38 ±0.13	-0.01 ±0.08	0.23 ±0.24
	C	tail	16.11	24.05	22.33	0.42 ±0.17	-0.02 ±0.10	0.18 ±0.20
Arp 245 [S+S]	A	galaxy	12.34	22.07	18.90	0.83 ±0.13	0.22 ±0.07	0.27 ±0.14
	B	galaxy	12.94	22.12	18.89	0.45 ±0.19	0.10 ±0.09	0.08 ±0.17
	C	tail	15.11	24.74	22.74	0.48 ±0.30	0.11 ±0.19	0.31 ±0.28
	D	bridge	15.69	24.56	23.45	0.65 ±0.18	0.23 ±0.12	0.33 ±0.18
	E	plume	14.32	23.65	22.35	0.67 ±0.11	0.15 ±0.06	0.29 ±0.13

TABLE II. (continued)

Object	Feature	Type	V_{26}	$\bar{\mu}$	μ_c	$B-V$	$V-r$	$r-i$
Arp 252 [S+S]	A	galaxy	15.60	22.45	19.50	0.56 ±0.09	0.10 ±0.13	-0.04 ±0.13
	B	galaxy	16.16	22.72	20.35	0.54 ±0.09	0.05 ±0.06	0.07 ±0.09
	C	plume	17.42	24.52	22.91	0.78 ±0.24	0.06 ±0.11	0.02 ±0.25
	D	bridge	17.43	24.08	23.02	0.53 ±0.15	0.00 ±0.07	0.14 ±0.10
	E	tail	16.68	24.28	23.09	0.72 ±0.21	0.00 ±0.09	0.23 ±0.21
Arp 295 [S+S]	A	galaxy	13.94	22.40	19.67	0.54 ±0.09	0.17 ±0.08	0.23 ±0.27
	B	galaxy	13.95	22.70	19.76	0.89 ±0.14	0.22 ±0.10	0.41 ±0.20
	C	bridge	16.24	24.86	19.75	0.61 ±0.42	0.13 ±0.18	0.43 ±0.38
	D	tail	16.53	24.69	22.67	0.51 ±0.29	0.15 ±0.18	0.30 ±0.30
Arp 319 [multiple]	A	galaxy	13.17	22.28	20.33	0.44 ±0.09	0.07 ±0.06	0.48 ±0.12
	B	galaxy	13.63	22.58	19.15	0.82 ±0.26	0.23 ±0.08	0.61 ±0.09
	C	galaxy	13.70	21.47	18.37	0.80 ±0.13	0.22 ±0.03	0.61 ±0.13
	D	galaxy	13.93	21.29	18.28	0.90 ±0.08	0.22 ±0.04	0.67 ±0.14
	E	tail	15.75	24.42	22.90	0.57 ±0.28	0.13 ±0.12	0.79 ±0.30

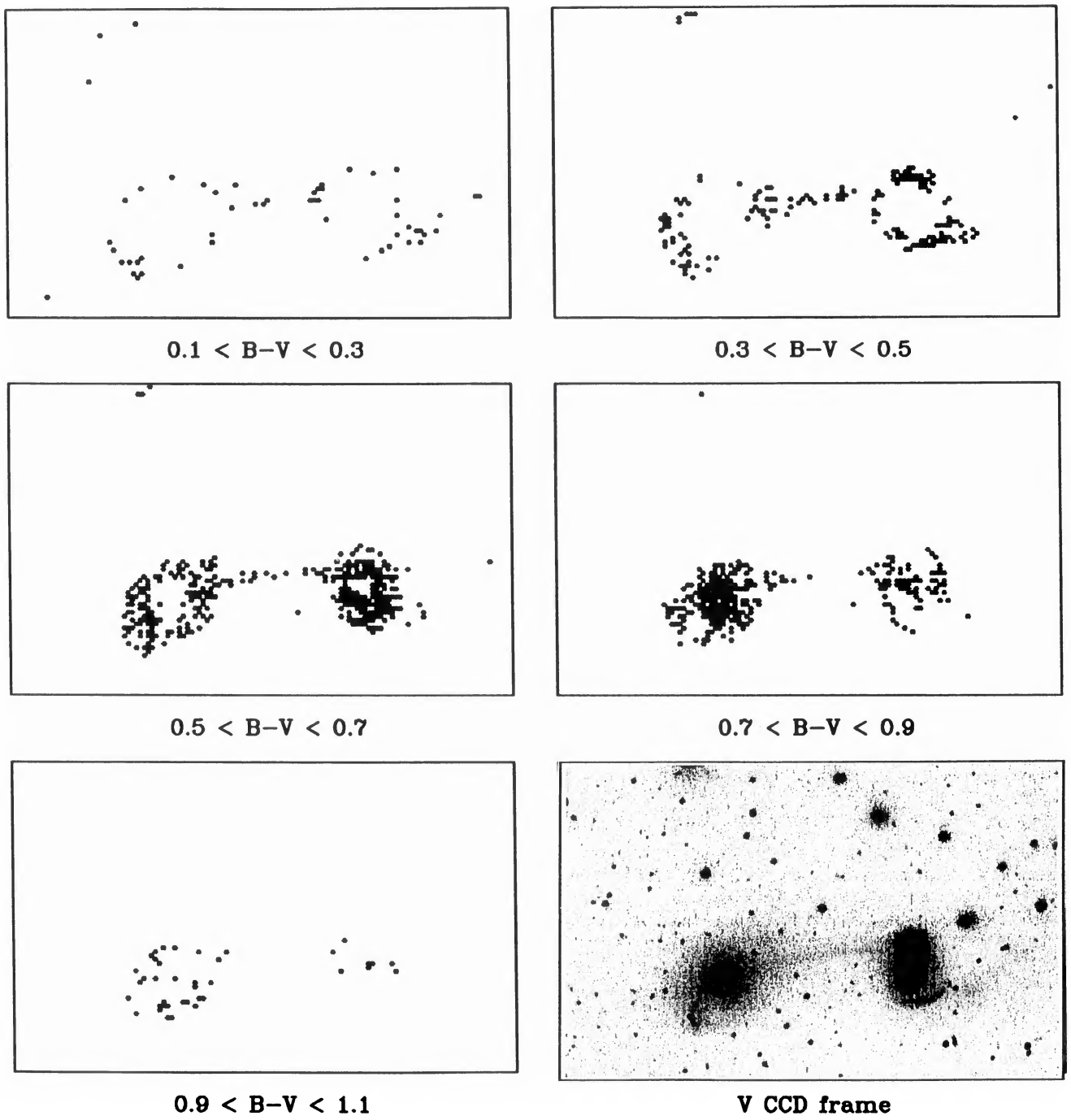

FIG. 1. Two-color grid photometry for Arp 104. Cuts of 0.2 mag in $B - V$ are shown from 0.1 to 1.1. Grey-scale 600 s V frame is also shown where north is right and east is up. The colors of all the tidal features are bluer than the central regions of either galaxy, but similar to the colors of the outer regions.

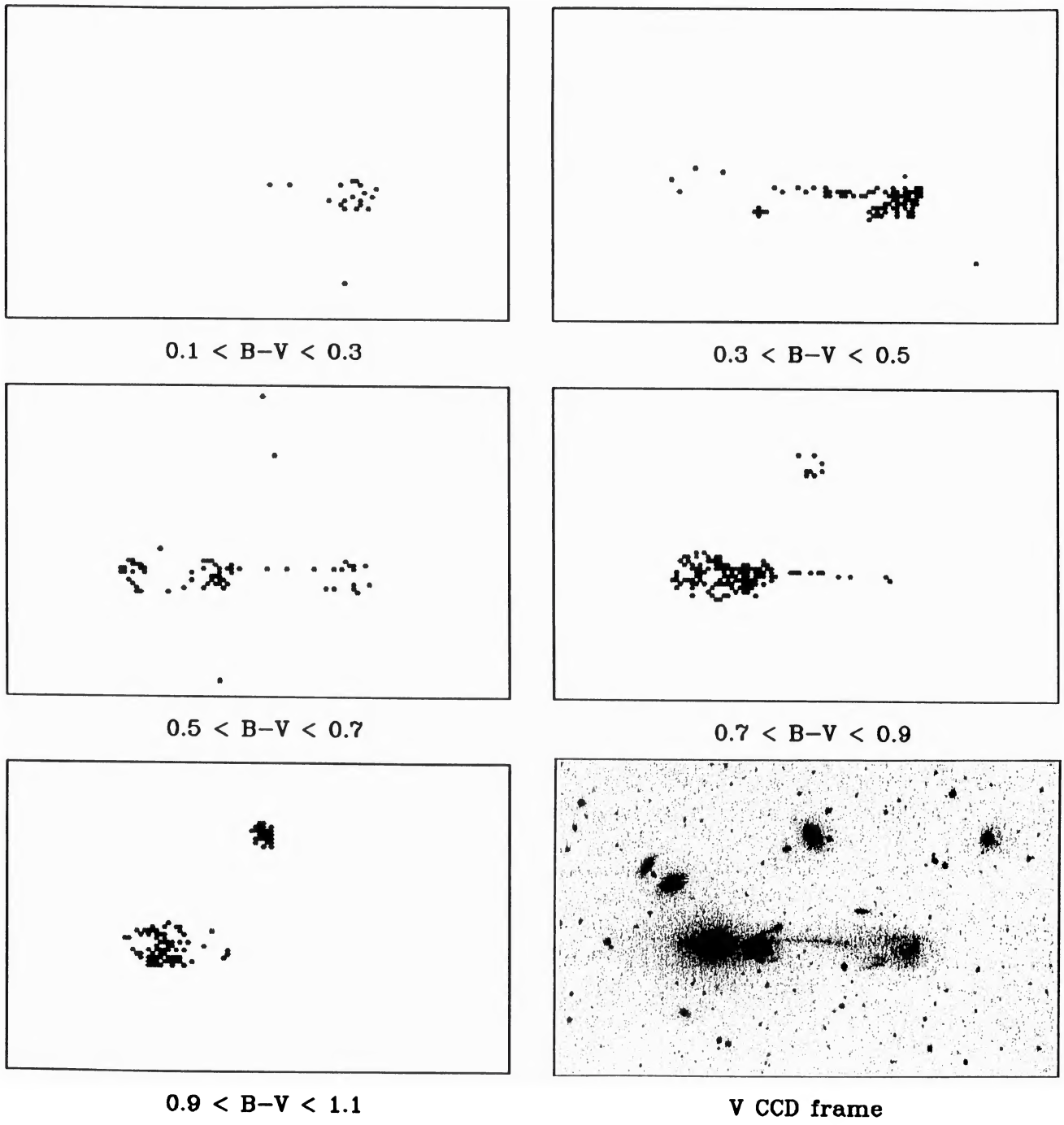

FIG. 2. Two-color grid photometry for Arp 105. Feature C, to the north, is faint in average surface brightness, yet extremely blue probably from a recent burst of star formation. The connecting bridge is also blue, although not to the extreme of feature C. There is also evidence of color gradients in both galaxies.

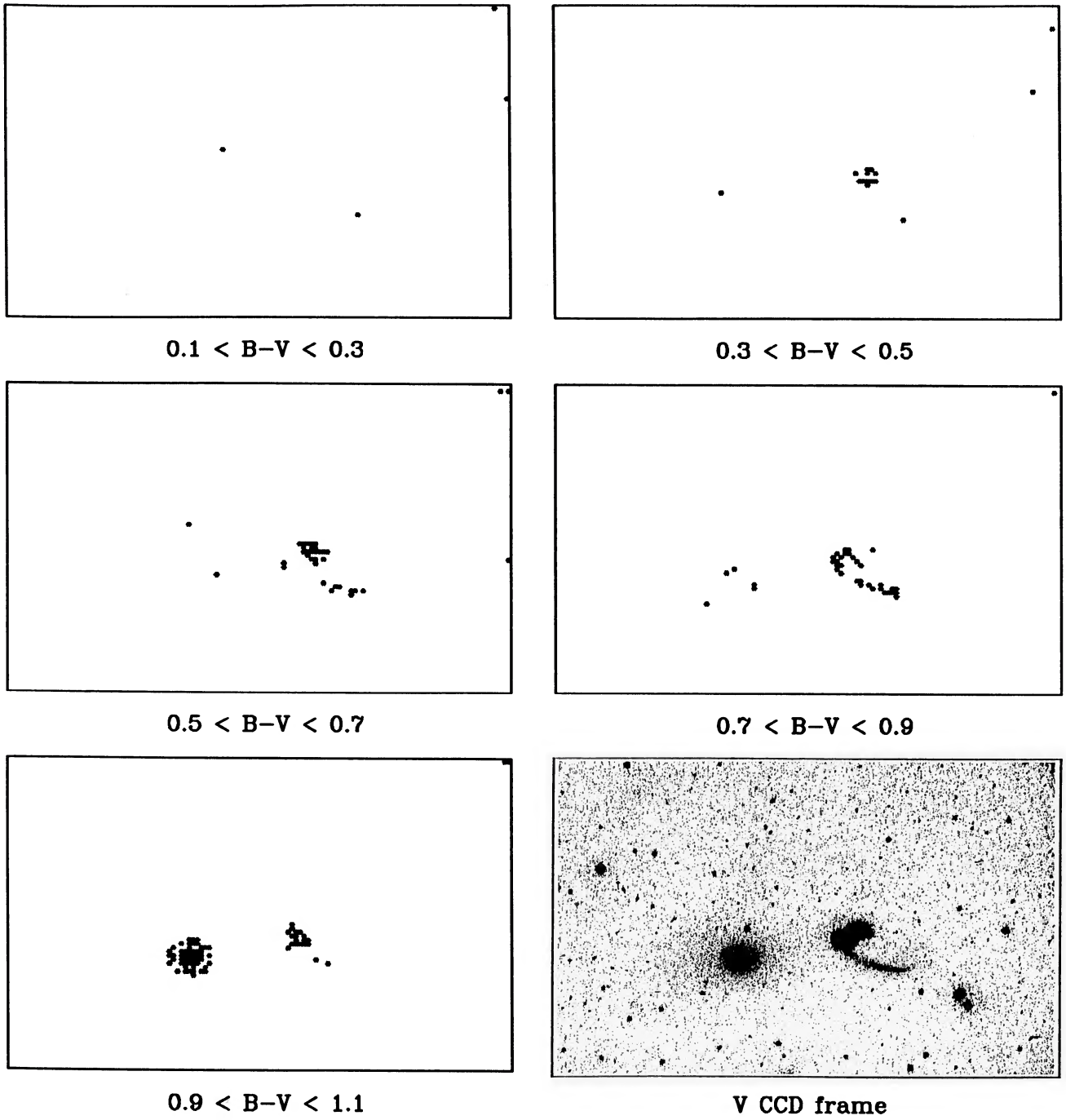

FIG. 3. Two-color grid photometry for Arp 190. The tidal tail to the northwest (feature D) is blue with distinct regions of star formation at its tip. It is clearly linked to the lower spiral, but is not an extension of a spiral arm.

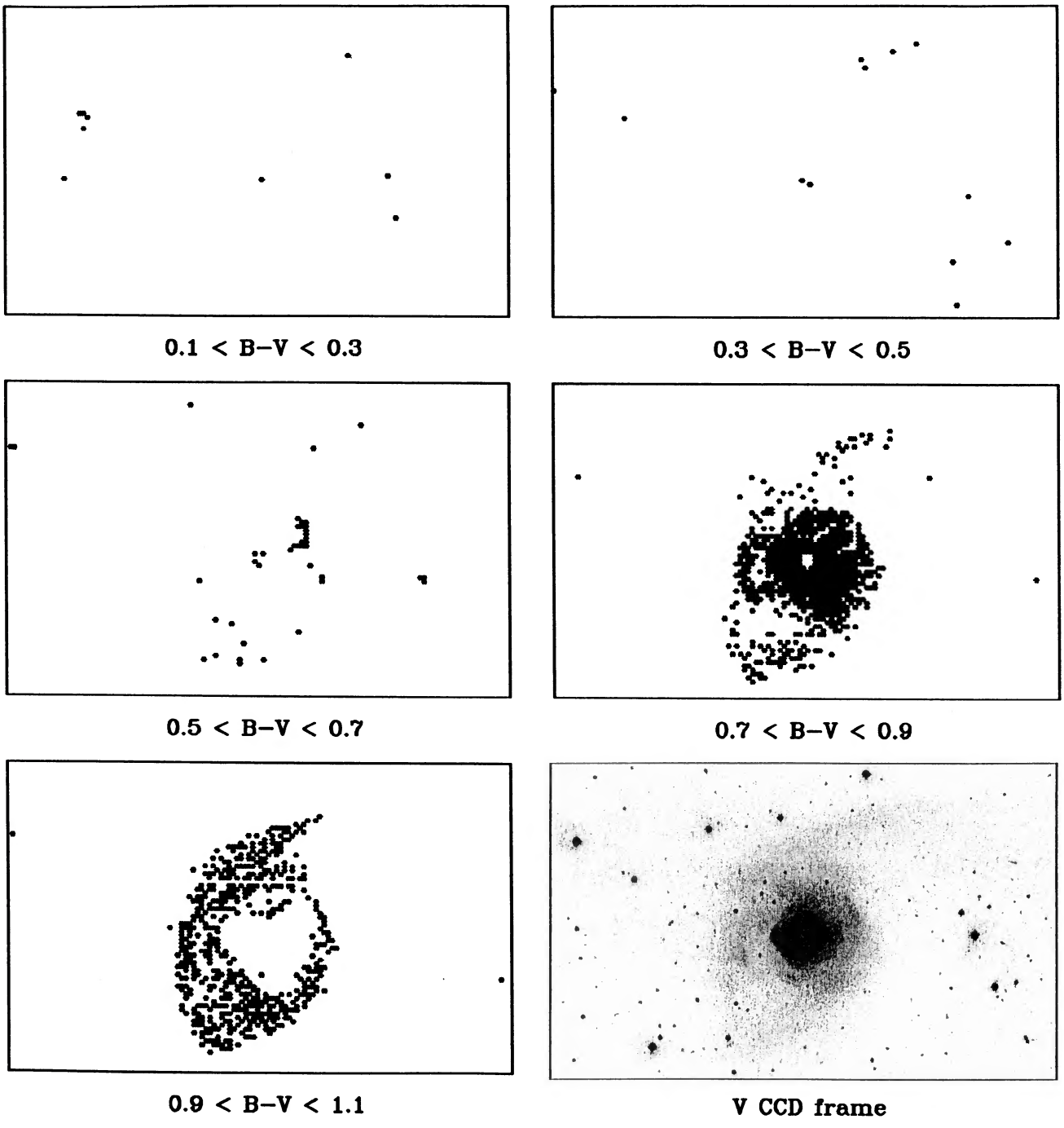

FIG. 4. Two-color grid photometry for Arp 222. There is a large range in color within the central body, but no evidence of strong star formation. The outer envelope is slightly redder than the mean color of the central body. Many of the shells and loops are bluer then the surrounding material which could imply a disk system which mergered with an elliptical or an S0. One particular loop is obvious as a blue hole in the $0.7 < B - V < 0.9$ slice.

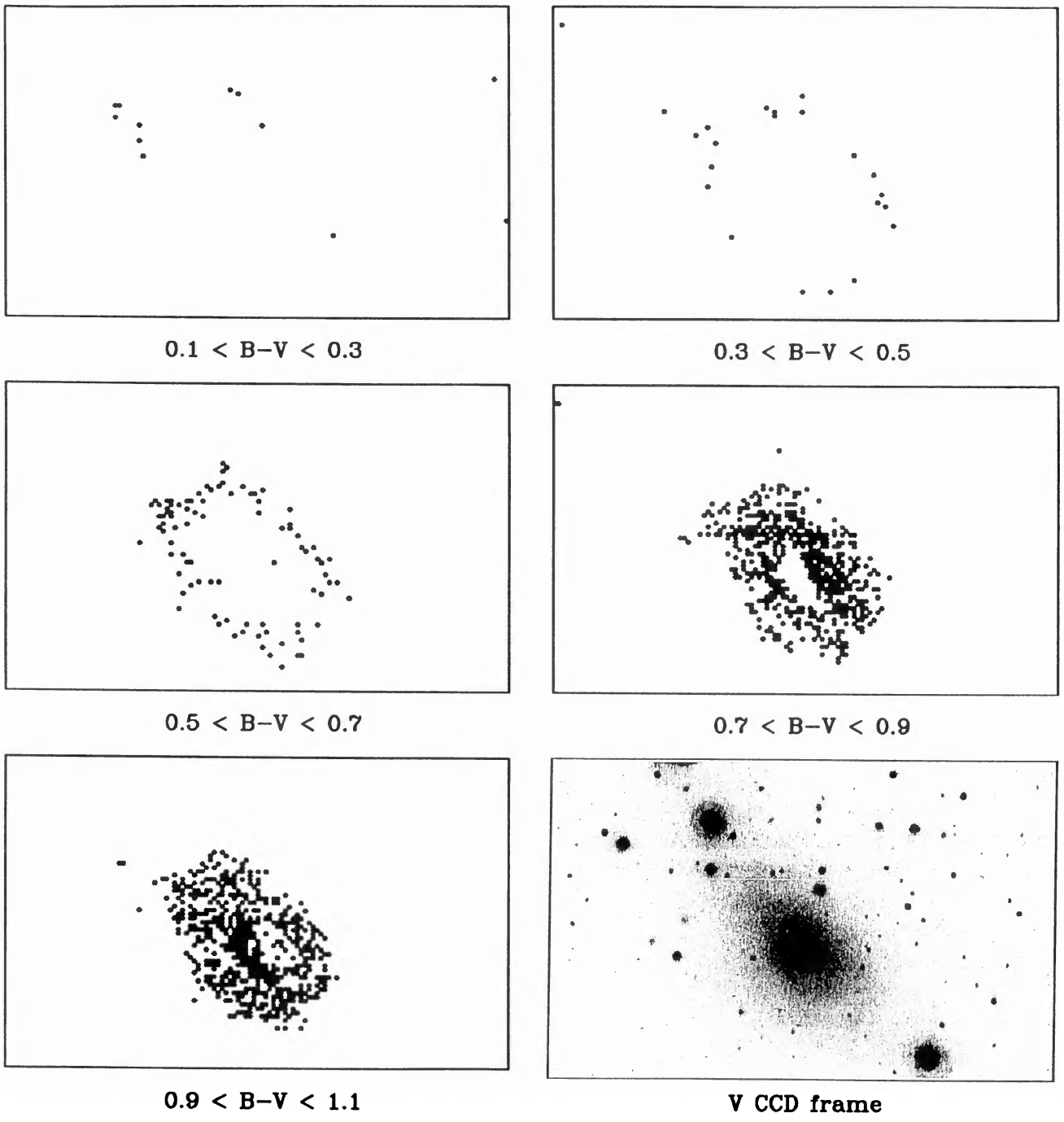

FIG. 5. Two-color grid photometry for Arp 232. The color map reveals that most of the disturbed structure in the V frame is the result of a dust lane which crosses below in major axis in a proto-Cen A fashion. Without the reddened dust region, the colors are typical of a early-type spiral, although chaotic spatially. This system demonstrates the strength of using two-color map to detect faint absorption lanes.

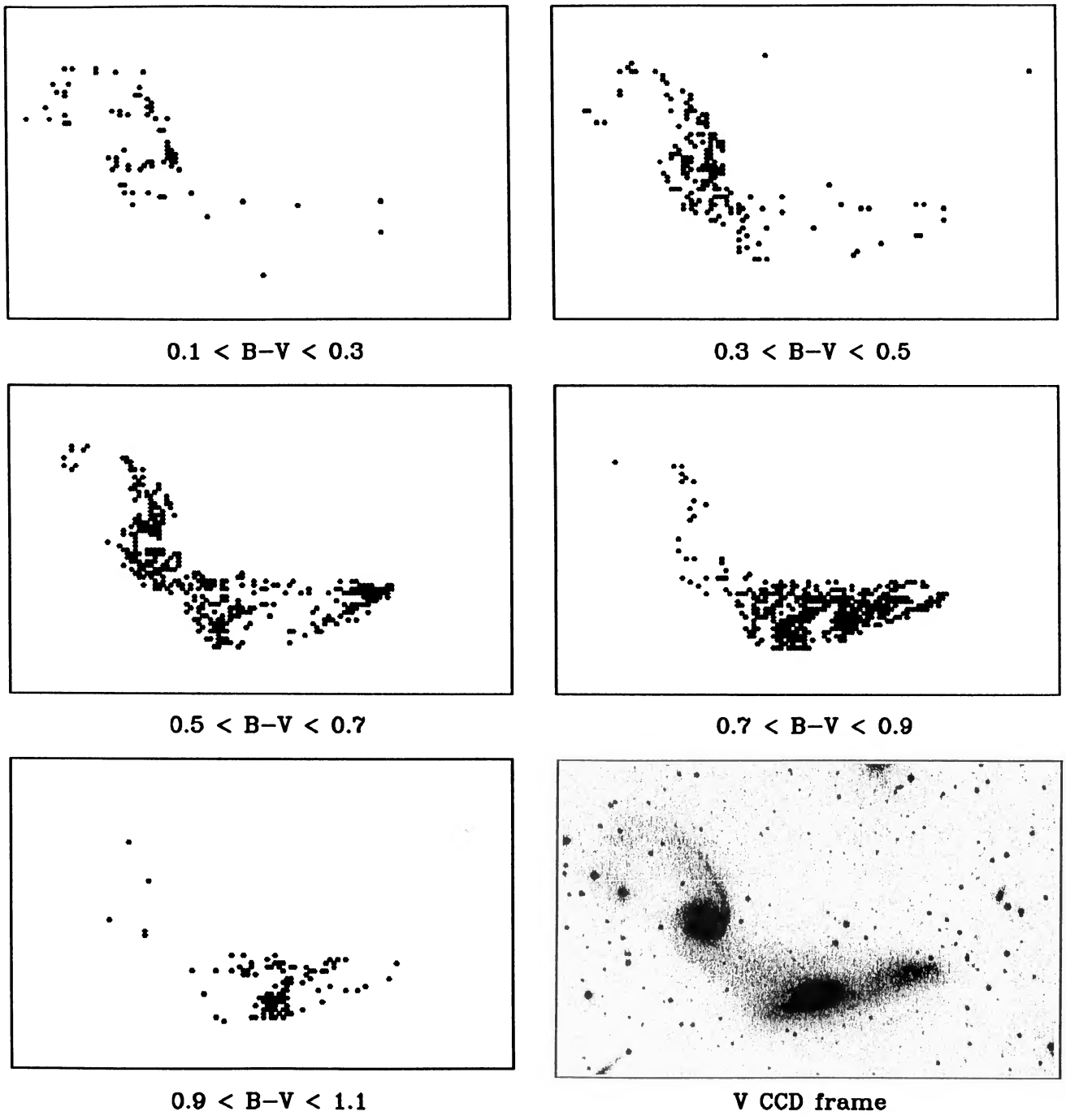

FIG. 6. Two-color grid photometry for Arp 245. The tail and plume display a great deal of resolved structure into star-forming regions in both luminosity and color maps. Since both features are very blue, either regions of star formation have been displaced by the disk or star formation has begun in these regions during the interaction.

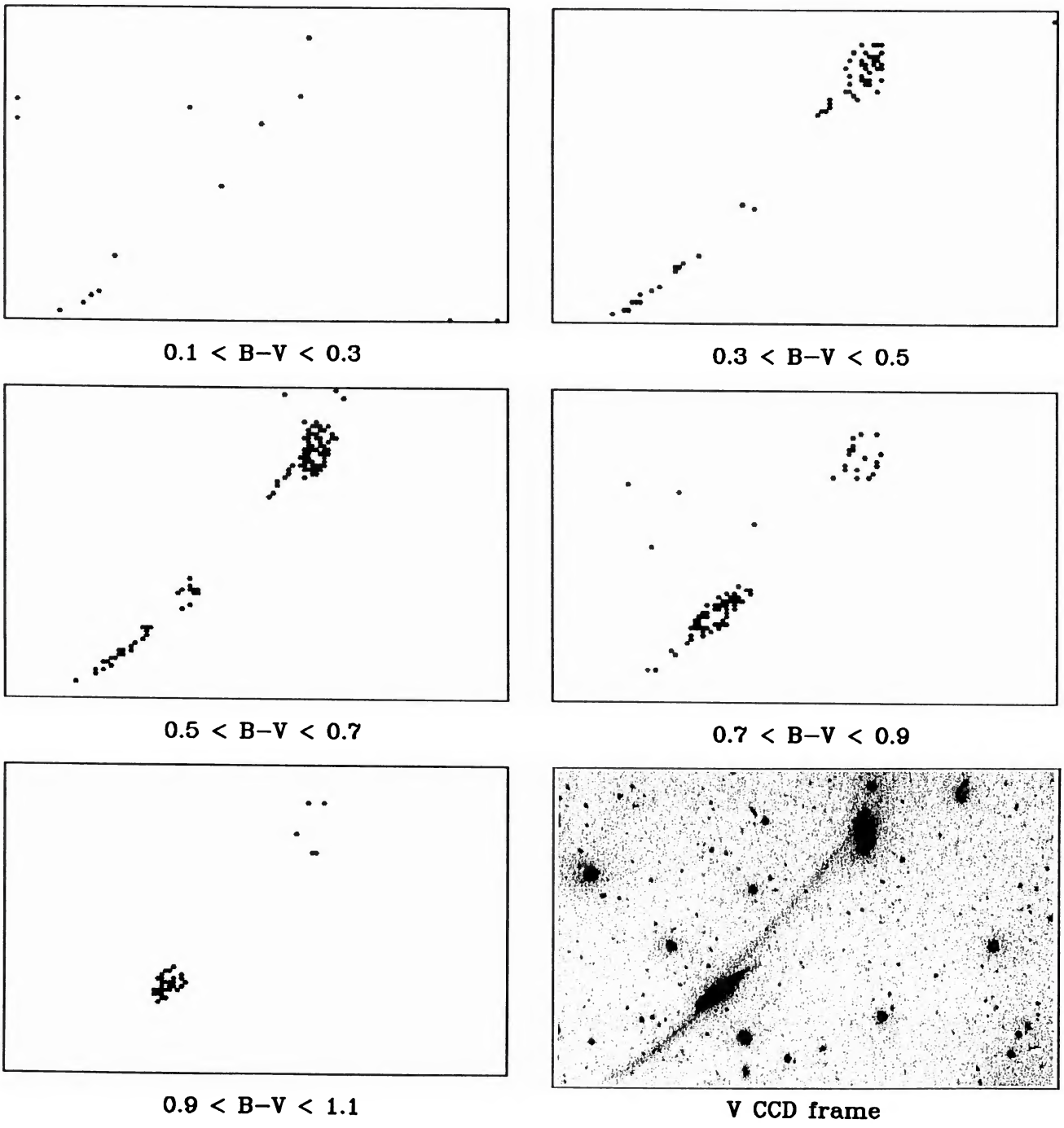

FIG. 7. Two-color grid photometry for Arp 295. The northern most galaxy still maintains some spiral structure, although the side with the connecting bridge feature is distorted. The southern galaxy is an edge-on Sb or Sc type. Its color structure is complicated by a central dust lane, but the outer regions are as blue as its companion. The two tidal features are a connecting bridge and a counter tail to the southwest. Both tidal features are blue ($R - V = 0.6$ to 0.5).

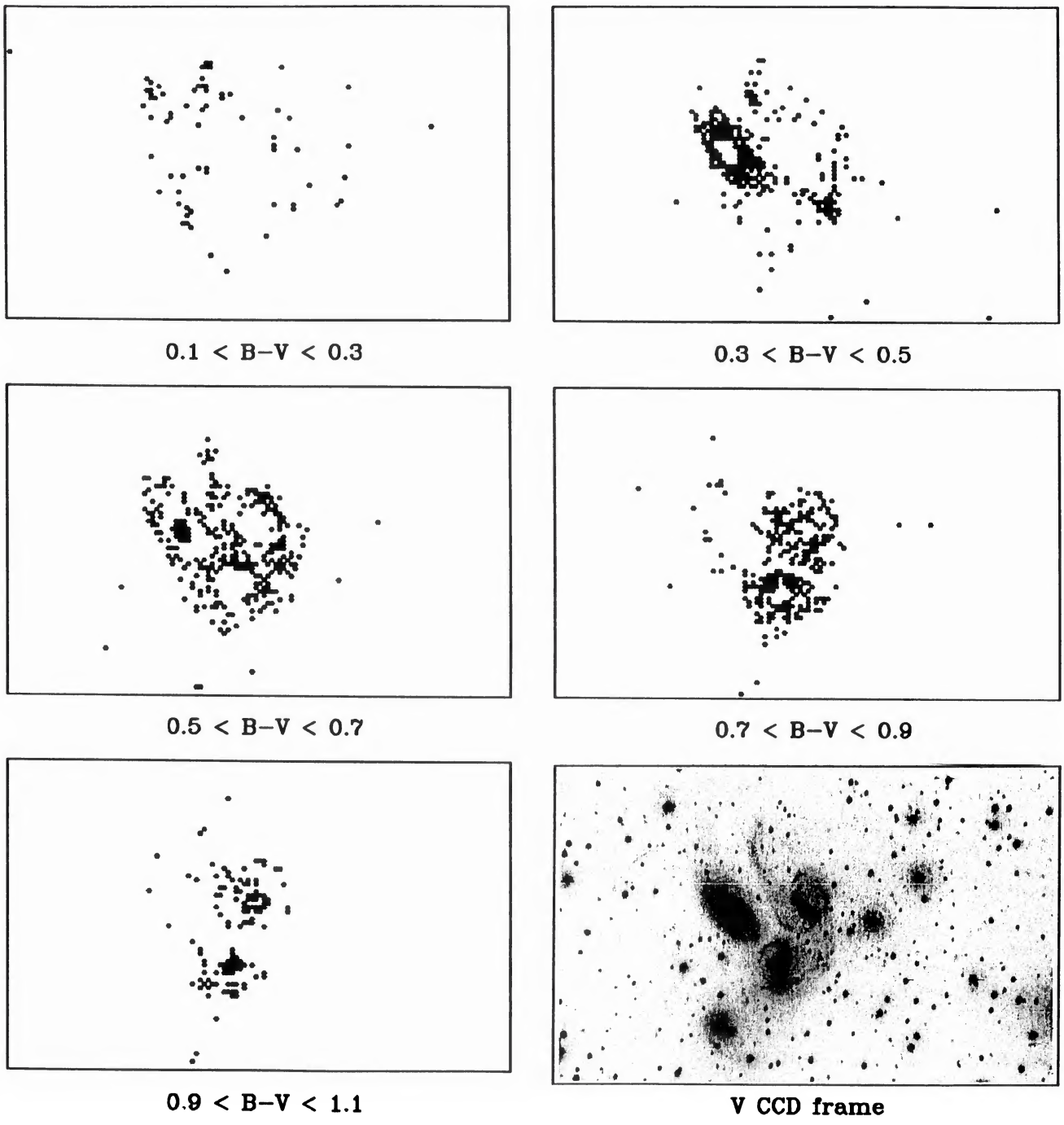

FIG. 8. Two-color grid photometry for Arp 319 (Stefan's Quintet). There is a common envelope in the intermediate regions between galaxies which has a blue color compatible with the outer disk colors of the spirals. The tail is blue ($B - V = 0.57$) and has the color, shape, and orientation that suggests it is an extension of an arm from a galaxy to the northwest rather than a tidal feature. There is a distinct grouping of H II regions to the north side of the system which is probably the remnant of a large section of material stripped from the spirals in this region.

b) Tidal Morphology

Tidal features discussed in this paper can be divided into six groups; tails, plumes, bridges, envelopes, shells, and loops. Our use of these terms, described below, may differ from common usage or descriptions in the Arp Atlas, and are intended only as a consistent scheme for this study only. It should be noted that classification was made from linear displays of CCD images rather than logarithmic photographic plate material. This has the disadvantage of de-emphasizing the contrast between outer galaxy light and tidal features, but has the advantage of identifying features deep in the interiors of galaxies, regions which are overdense on photographic plates, and allowing for interactive clipping and contrast control to search for new features.

The reduction procedures were designed to treat each of these tidal features in a similar fashion. However, simply because of their differing geometry, certain groups are easier to analyze by being more isolated from the parent or primary galaxy. For example, tails, plumes, and bridges are easy to separate from primary galaxies compared to envelope or shells because they extend well beyond the galaxy edge and are little effected by contamination. Envelopes, on the other hand, require some choice be made on where the galaxy stops and where the envelope begins. The results of the classification, and based on visual examination of the CCD frames, are listed in Table II according to the definitions described below.

Tails were defined to be those linear structures that have an origin at the edge or within a primary galaxy. A tail does not make projected contact with any other galaxy, nor does it loop back onto the primary galaxy (or else it would be a loop). Tails are usually higher in surface brightness than other tidal features (a fact which may be related to viewing angle, see Sec. IV). They are also narrow with sharp, well-defined edges in cross section.

Plumes have most of the characteristics of tails; separate identity from the primary galaxy, though connected to its primary galaxy, and is not in projected contact with any other object. However, as the name suggests, plumes are lower in surface brightness and have a more diffuse appearance. They differ from tails in that they do not have a well-defined ridgeline nor do they have sharp edges. Plumes tend to be more folded or curved along the long axis than tails, which are usually very straight.

Bridges are simply defined to be any linear feature which connects two galaxies. If no dynamical models were available, it would somewhat surprising to find that bridges were always similar in shape and cross section to tails. From previous dynamical models, it is likely that these similarities result from both the similar dynamical processes that formed them and the projection effects that cause the features to be classified as tails and bridges (TT). Without these models, it would be easy to believe that bridges are simply tails projected onto the companion. In addition, there is a very sharp correlation between the angle of the bridge and the line of centers of the galaxies with no examples of bridges with angles slightly off center.

Envelopes are defined to be a symmetrical luminosity pattern that surrounds two interacting galaxies (i.e., Arp 169) or a halo in a system with other evidence of disturbance (Arp 223). All envelopes are, by nature, low in average surface brightness, but are not uniform in distribution such as cD galaxies. There are usually distinct regions of high and low surface brightness within an envelope but lacking the radial symmetry or sufficient independence from the rest of the luminous matrix to warrant a plume or tail classification. And, there are often shells and loop structures embedded in envelopes (see below). Envelopes were only found in elliptical plus elliptical systems or merger remnants.

Last, there were many incidences of shells and loops in the sample. Shells or ripples are sharp-edged, partially circular features usually seen on top of envelope or galaxy light (Malin and Carter 1983). Loops are thin, ridgeline, arc features also seen embedded within galaxies. The difference between shells and loops are that shells have a plateau appearance in cross section (i.e., constant intensity with a sharp edge); whereas loops are Gaussian shaped in cross section (i.e., a bump in the underlying light); however, unlike a shell, they are rarely radially symmetric about the primary center. For the most part, since shells and loops were deep within the primary galaxy luminosity, they were excluded from the analysis. But, particularly interesting examples are discussed in Sec. IIIc and the general issue of shells or ripples has been discussed in Schombert and Wallin (1987), Schweizer and Seitzer (1988) and modeled by Hernquist and Quinn (1989, and references therein), and Wallin (1989).

c) Individual Objects

By design, the objects selected for this sample form a cross section representative of most types of interacting system. We feel that a short discussion of each object is helpful, if only to identify the features listed in Table II. The reader is encouraged to skip the following section and only return to these comments as needed. A copy of the Arp Atlas aids in reviewing the following descriptions.

1) Arp 96

At first glance, the Arp 96 system could easily be mistaken for a chance projection of two galaxies rather than a true interaction. The connecting bridge and northern plume appear to be natural extensions to the primary galaxy's spiral structure. However, on closer examination, the two tidal features show distinct contours separate from the spiral arms. The primary galaxy (object A, a Sbc type spiral) has slightly tighter arms with the bridge and plume originating at the points were the pitch angle changes. The northern plume (referred to as feature C in Table II) is a counter-tail under the normal interpretation from collision models. The southern feature (feature D) is a connecting bridge to the southern elliptical companion. The bridge axis is directly oriented toward the elliptical's (object B) center. In addition, there is an extremely faint shell feature (not analyzed) to the southwest of the elliptical which substantiates the interaction interpretation for this pair. The colors of the tidal features are, within the errors, identical to the colors of the outer areas of both galaxy A and B. This is as would be expected if the material in the tidal features are simply stellar debris removed from the red galaxies themselves. No evidence for any star formation is detected in either the color maps (i.e., no isolated blue regions) or the as high-surface-brightness peaks in the V frames.

2) Arp 97

This system appears to be two interacting ellipticals; however, the colors of the southern galaxy (object B) are more indicative of a Sbc or Sc spiral. The interaction has destroyed

any clear disk structure from either galaxy. The connecting bridge (feature C) is similar in color to galaxy B, bluer than the elliptical galaxy (object A). The southeastern plume (feature D) is very blue ($B - V = 0.39$) and has visible knots of star formation. It is unclear in this example whether the star formation is tidally induced or whether the disk of galaxy B has been disrupted to form two features.

3) Arp 100

The two galaxies in Arp 100 are more widely separated relative to the other systems in this sample. The southern object (object B) appears elliptical and shows no evidence of distortion in its isophotes. The spiral (object A) to the north shows extreme disruption with little coherent structure. A northern tail (feature C) is high in surface brightness as compared to other tidal features, a trait common to tails versus plumes, and may be related to the geometry with respect to the line of sight of these types of features. The southern plume (feature D) is fainter, but is of the same blue color as the tail implying common material for their origin. The primary galaxy A has a red core with a blue gradient that matches the colors of the tidal features. In fact, Arp 100 is one of our first examples of a system where the mean colors of the tidal features are bluer than the primary galaxies, yet match the outer disk colors exactly. The interpretation here is that the tail and plume are outer regions of galaxy A that have been pulled out and are viewed with different lines of sight resulting in different mean surface brightnesses, yet similar total luminosities for the features.

4) Arp 101

Similar in appearance to the Arp 100 system, the Arp 101 system consists of two red galaxies, a southern elliptical (object B) and a northern disk galaxy (object A). Galaxy A is probably a distorted Sa type with a northwest tail (feature C) and a southeastern plume (feature D). The tail feature C is a good example of this type with a narrow, high-surface-brightness "stem" with a sharp fall off in brightness on each side (see Fig. 8). The plume feature D almost crosses to galaxy B, but there is a sufficient drop in luminosity to classify it as a plume rather than a bridge. The isophotes of galaxy B are distorted in the direction opposite to galaxy A. Both tidal features are bluer than the primary galaxies, yet their structure is quite smooth with no obvious regions of star formation.

5) Arp 102

Arp 102 is also an elliptical/spiral interaction, but the tidal features are more distorted and fragmented than the previous examples. The northern spiral (object A) has a red average color in Table II; however, there is a very strong blue gradient such that the outer disks colors match the tidal feature colors. The southern elliptical (object B) appears quite normal in structure and color. The northern plume (feature C) is very blue, with many high-surface-brightness regions of star formation. In general, the structure of the tail is much more complex than simpler tails (e.g., feature C in Arp 101). The tail is divided into two sections by an absorption band and gives the basic appearance of a spiral structure that has been removed and straightened by the interaction. The connecting bridge (feature D) is also blue, but fainter and smoother. There are also several faint features around galaxy A, such as loops of luminous material to the northwest and small, linear segments to the south.

6) Arp 103

The two primary galaxies in Arp 103 appear to be elliptical or S0-like objects. The red colors ($B - V = 0.8$) confirm the late-type classification. However, deeper examination of the blue CCD frames reveals a pattern of dust lanes in the southern (object B) and shells around the northern companion (object A). There is a slight color gradient in object B and it may be a later type spiral (Sab or Sb). The connecting bridge (feature C) is slightly bluer, but compatible with the colors of the outer regions of object B. There are several distinct knots in the bridge (i.e., possible sites of star formation). The object to the southwest of object B is highly distorted, but appears to be a background galaxy or companion disk galaxy rather than a tidal feature.

7) Arp 104

The northern galaxy (NGC 5216, object A) is severely disturbed. It has both a tidal plume (feature C) to the north and a bridge (feature D) to the south, although neither is structurally related to any spiral feature in galaxy A. The southern galaxy is an elliptical (NGC 5218, object B) with a small tail to the southwest (feature E). There is slight evidence of non-elliptical distortions in its isophotes. The connecting bridge is oriented directly at the center of the elliptical and is very narrow and well-defined. The colors of all the tidal features are bluer than the central regions of either A or B, but similar to the colors of the outer disk of A (see spatial color map in Fig. 1). Considering their smooth appearance (i.e., the lack of any distinct star-forming regions), a scenario where material is removed from the disk of galaxy A is plausible.

8) Arp 105

Arp 105 is spectacular in its suggestion of a collision where a disk has been removed, practically intact, from one of the interacting pair. The two primary galaxies are a severely distorted spiral (object A) near an elliptical (object B). Two arcminutes to the north lies a roughly circular pile of material (feature C) which has several distinct groupings of luminous material. There is the suggestion of symmetry about the brightest region in this pile. Last, there is a connecting bridge (feature D) between A and C. Feature C is faint in average surface brightness, yet extremely blue probably from a recent burst of a star formation (see Fig. 2). The connecting bridge is also blue, although not to the extreme of feature C. There is also evidence of color gradients in both A and B.

9) Arp 169

The extended feature in the Arp 169 system is the first example of what will be called a tidal envelope. There can be little doubt that the two ellipticals (northern elliptical is object A, the southern is object B) are interacting. Their isophotes are strongly distorted and elongated towards each other. The surrounding envelope (feature C) is smooth and concentric to the center of mass of the pair. There are enhanced regions of luminosity on opposite sides of the ellipticals and in the region between them. There are also faint shell-like edges in the outer regions. A high contrast image of the system suggests that the envelope could actually be di-

vided into two separate plumes, but the lack of a definitive boundary requires that the envelope be analyzed as a whole. The colors of the envelope match the colors of the ellipticals with no evidence of color structure or gradient. We are probably witnessing an early stage of a merger, where the velocities between the objects are low and the angular momentum vectors are oriented such that large tidal features do not form.

10) Arp 170

Similar to the Arp 169 system, the Arp 170 system is another example of an interaction (possible merger) between two ellipticals. Again, the isophotes of both galaxies (the northern elliptical is object A, the southern is object B) are distorted and twisted towards each other as expected for a close interaction. The surrounding envelope (feature C) is stronger around galaxy B in the inner regions, but becomes much smoother and concentric to the center of mass at large radii and fainter light levels. The envelope is the same color as the two ellipticals with no evidence of recent star formation.

11) Arp 172

Both galaxies in the Arp 172 would be classified by eye as ellipticals. They are relatively smooth and red with no evidence of dust or gas. The southern galaxy (object B) is strongly distorted with nonconcentric isophotes and several lumps along its major axis. The northern galaxy (object A) has smoother contours, but still displays distortions in its outer contours. There are two plumes in this system, opposite in orientation and shape. The northern plume (feature C) is very broad and red ($B - V = 1.00$). The southern plume (feature D) is slightly narrower, but also very red ($B - V = 1.02$). This system has the suggestion of being a younger version of the extended envelopes from the previous two examples, where the plume material has not yet relaxed into a common envelope and retains separate identities. However, a difference in angular momentum or impact parameter of the interaction could also account for the differences between two plumes or a common envelope. And, the strength of the interaction must be high in order to split the core of the southern galaxy.

12) Arp 173

Arp 173 is an example of a system with a very sharp and well-defined tidal tail. The two galaxies are very distorted and classification is impossible; however, their colors suggest they are star-forming, gas-rich systems. The northern galaxy (object A) is very irregular and high in surface brightness. It has patches of red and blue regions similar in appearance to the nearby Irr NGC 4449 (Thronson *et al.* 1987; Bothun 1986). It also has an loop of faint material on its eastern side and several other small plumes to the west and south. The southern galaxy (object B) is also disturbed and unclassifiable from its structure and has very blue colors suggesting a current phase of star formation. The tidal tail (feature C) is very sharp in cross section and, although there are no obvious regions of star formation, its colors are also very blue.

13) Arp 179

Arp 179 is the only object in this sample which does not clearly have a companion galaxy to support the interaction hypothesis for tidal features, although the companion could be behind the system. Arp 179 may also be a pair of galaxies which are in the process of merging. Similar examples of this type of system have been seen by Schweizer (1986). The tidal tail (feature B) is similar to other tails in this study, although somewhat fainter in average surface brightness and less sharply defined at its edges. The central galaxy (object A) is a disk system with $B - V$ colors similar to a Sb class spiral. The tail is, within the errors, the same color as the galaxy.

14) Arp 190

Arp 190 is a triple system. Although not visible in the Arp Atlas, there is a connecting bridge between the lower spiral (object B) and the southern elliptical (object C). The northern spiral (object A) may be projected onto the system since its structure is undisturbed. The tidal tail to the northwest (feature D) is blue with distinct regions of star formation at its tip. It is clearly linked to the lower spiral B, but is not an extension of a spiral arm. The bridge (feature E) is smooth and similar in color to the elliptical. Figure 3 shows the spatial color map for the system.

15) Arp 193

One of the strongest *IRAS* sources in the northern sky, Arp 193, has the appearance of a merger in the late stages of evolution. The central object (object A) has several distinct nuclei, but positive identification of the original galaxies is impossible. Its colors are quite blue ($B - V = 0.4$) and there is clear evidence of an extreme amount of star formation. The two tails, southwest (feature B) and southeast (feature C), are very irregular with several H II regions and as blue as the central body itself.

16) Arp 204

The objects in Arp 204 are so disturbed that separation into primary galaxies and tidal features is difficult. The easternmost galaxy (object A) retains some of the appearance of an edge-on spiral, probably of the Sc type. However, its outer regions are strongly distorted. At the western edge of the system lies a clump of faint material with a nucleus that is identified in Table II as object B. Southeast of the nucleus is a tail of material (feature C) which has several collections of H II regions aligned to the galaxy. Last, there is a faint, disordered bridge between A and B (feature D). Both tidal features are extremely blue and show signs of star formation. The interpretation presented here is that a late-type spiral (the remnant of which is object B) was disrupted to form the tidal features.

17) Arp 222

Objects, such as Arp 222, display a structure that is very complex, showing shells, loops, and distorted isophotes. The central body in Arp 222 (also known as NGC 7727) has a distinct nuclear region with no evidence of multinuclei. However, the isophotes are non-elliptical and nonconcentric. There are many low-surface-brightness shells and loops within the envelope, symmetric to the nucleus. There is a large range in color within the central body, but no evidence of strong star formation. The outer envelope is slightly redder than the mean color of the central body. Many of the shells and loops are bluer then the surrounding material which could imply a disk system which merged with an ellip-

tical or an S0. One particular loop is obvious in Fig. 4 as a blue hole in the $0.7 < B - V < 0.9$ slice.

18) Arp 223

Arp 223 is similar to Arp 222, but its contours are less disturbed and more elliptical-like. The colors of the central region also complex with a mean $B - V = 0.93$, slightly bluer than a normal elliptical Arp 223 is asymmetric in color with the west side being redder by ≈ 0.05 in $B - V$. This is possibly the combined effect of a dust lane and the inclination of the object (implying it is an S0). There are several shell features embedded in the envelope, many of which are bluer then the envelope itself. The interpretation is that Arp 223 is a slightly more evolved system than Arp 222, where the motions have had time to virialize and any thin features have been destroyed.

19) Arp 232

Arp 232 was selected for this project because of the non-elliptical appearance of its isophotes suggesting a recent merger. However, inspection of its color map (Fig. 5) reveals that most of the disturbed structure is the result of a dust lane which crosses below in major axis in a proto-Cen A fashion. Without the reddened dust region, the colors are typical of an early-type spiral, although chaotic spatially. This system demonstrates the strength of using two-color maps to detect faint absorption lanes (see Barsony 1988).

20) Arp 242

One of the original systems presented by TT as a classic example of a tidal interaction is Arp 242. Both the northern galaxy (object A) and the southern galaxy (object B) have the shape and colors of early-type spirals, although the disk regions are strongly distorted or absent. The northern tail (feature C) has sharp edges and a well-defined high-surface-brightness ridgeline. The southern plume (feature D) is lower in surface brightness and less well-defined at the edges. Both features are bluer than the primary galaxies central colors, but in agreement with the colors of outer-disk regions.

21) Arp 243

Similar to Arp 193, the scenario for Arp 243 is two gas-rich galaxies in the final stages of merger. The central body (object A) is very complicated in structure and color and cannot be separated. There are two large concentrations of luminosity to the north and south sides of the central mass, assumably the remnants of the original galaxies. The center colors are quite blue ($B - V = 0.3$–0.5) with strong evidence of ongoing star formation. The two tidal tails are on the east (feature B) and west (feature C) side of the central body. Each has also has very blue colors and distinct regions of star formation.

22) Arp 245

Arp 245 is one of the closest system in this sample, and provides the highest signal-to-noise plus resolution for color analysis. The northern galaxy (NGC 2992, object A) has extremely complicated and disturbed structure plus a color distribution that indicates strong absorption by dust. The southern companion galaxy (NGC 2993, object B) is much bluer than galaxy A, despite its similar morphological appearance, probably because it is face-on and less reddened by dust. There are three tidal features, a southern tail (feature C), a connecting bridge (feature D), and a northern plume (feature E). The bridge is smooth and faint in surface brightness, but blue ($B - V = 0.65$). The tail and plume, in contrast, display a great deal of resolved structure into star-forming regions in both luminosity and color maps (see Fig. 6). Both features are very blue. Either regions of star formation have been displaced by the disk or star formation has begun in these region during the interaction.

23) Arp 252

The two galaxies in Arp 252 are severely distorted, possible late-type spirals of Sc or Sd class. The northern galaxy (object A) displays the remnant of a disk and bulge with a plume to the northeast (feature C) and a connecting bridge (feature D) to the southern galaxy (object B). The southern galaxy appears as more of a knot of high-surface-brightness material between the bridge and a southwestern tail (feature E). The plume and the bridge are clumpy with colors that match the outer regions of the galaxies. The tail is smooth and sharp edged with a slightly redder color than galaxy B.

24) Arp 295

The two galaxies in the Arp 295 system are more widely separated than typical for this sample. The large separation and the narrowness of the features indicate that this system is probably seen nearly edge-on. The size of the system indicates the viewing angle must be nearly perpendicular to the plane on which the two galaxies lie. The northern most galaxy (object A) still maintains some spiral structure, although the side with the connecting bridge feature is distorted. The southern galaxy (IC 1505, object B) is an edge-on Sb or Sc type. Its color structure is complicated by a central dust lane, but the outer regions are as blue as its companion (see Fig. 7). The two tidal features are a connecting bridge (feature C) and a counter tail (feature D) to the southwest of galaxy B. Both tidal features are blue ($B - V = 0.6$ to 0.5).

25) Arp 319

Arp 319, commonly known as Stefan's Quintet, is a complex interaction between four spirals (the fifth spiral on the southwest side is not a member of the group) and represents an extreme end of the interaction scenario. Starting with the southernmost spiral and progressing clockwise the four spirals are marked as A, B, C, and D in Table II. A tidal tail to the east was also selected for analysis and is marked as feature E. Galaxy A is the bluest of the set, galaxies C and D are strongly distorted with the loss of one spiral arm for each. There is a common envelope in the intermediate regions which has a blue color compatible with the outer disk colors of the spirals (see Fig. 8). The tail is blue ($B - V = 0.57$) and has the color, shape and orientation that suggests it is an extension of an arm from galaxy D rather than a feature from galaxy B. There is a distinct grouping of H II regions to the north side of the system which is probably the remant of a large section of material stripped from C and D.

IV. DISCUSSION

a) Structure

The interacting systems in this sample fall into one of four categories: elliptical plus spiral (E + S, eight systems), ellip-

tical plus elliptical (E + E, three systems), spiral plus spiral (S + S, seven systems), and merger remnants (six systems). Overall, 43 tidal features were isolated for analysis as listed in Table II; 17 tails, ten plumes, 11 bridges, and five envelopes. Sharp tidal features, tails and bridges, were more common in E + S or S + S interactions, whereas diffuse features such as plumes and envelopes were most often found in E + E and merger systems. Bridges were slightly more common in E + S systems and tails dominated S + S systems. This supports the impressions one gets from the Arp Atlas images, and the conclusions from TT that the internal velocity dispersion from where the material originates strongly dominants the appearance of the tidal feature. That is, sharp features originate from "cold" disks (i.e., low velocity dispersion) and broad, diffuse features originate from "hot" components (i.e., ellipticals). And, the occurrence of specific tidal features matches well with the collisional interpretation in terms of the orientation and shape along the long axis. Ellipticals in this sample were more resistant to the formation of thin tidal features compared to spirals (e.g., Arp 169 and Arp 170). In the cases where bridges connected an elliptical with a spiral, the colors indicate that the bridge material had its origin with disk material in the spiral (e.g., Arp 96 and 190). Thus, we find that *blue, thin tidal features are stripped disk material; whereas, the diffuse, red features are from dynamically hot components, bulges, and ellipticals.*

The intensity cross sections of the tidal features divide into two categories; Gaussian-shaped and plateau-shaped profiles. Four examples are shown in Fig. 9. Tails and bridges were always smooth and Gaussian in cross section. Plumes were usually plateau shaped, rising quickly to a level of constant surface brightness across most of the feature. The definition of plumes versus tails and bridges is based in part on this division in cross sectional shape. Plumes are called plumelike because of their intrinsic diffuse nature; whereas, tails and bridges are defined to be narrow and sharp in surface brightness. However, it should be noted that these cross sections suggest that the tails and bridges are either thin and stringlike or edge-on sheets, and plumes are near face-on sheets. This, of course, assumes that tidal features are opti-

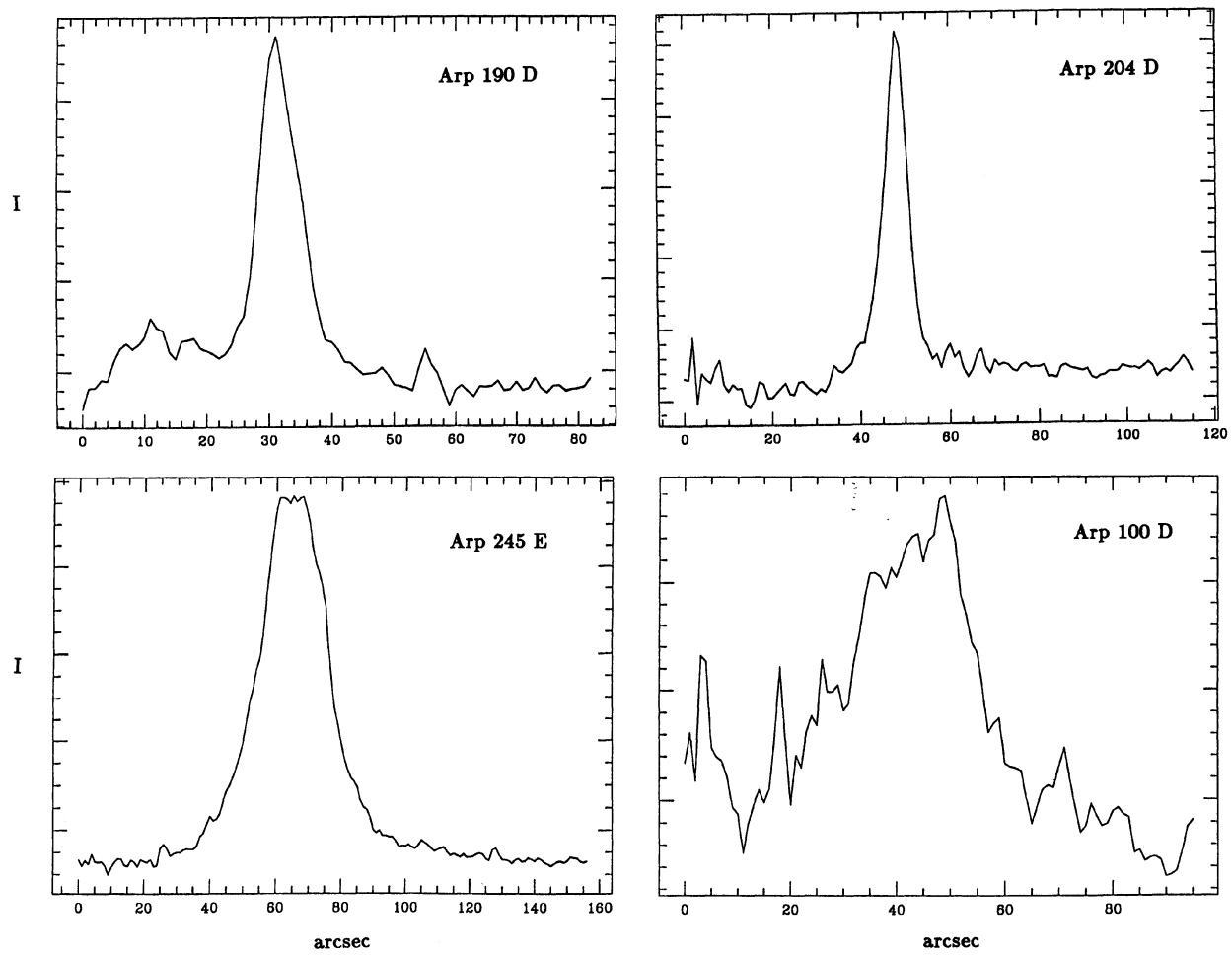

FIG. 9. Intensity cross sections for four tidal features. The top panels are a tail and bridge feature. The bottom panels are two plume features. In general, tidal features divide into two types: Gaussian-shaped and plateau-shaped profiles. Tails and bridges were always smooth and Gaussian in cross section. Plumes were usually plateau shaped, rising quickly to a level of constant surface brightness across most of the feature.

cally thin and dust or gas obscuration is not the cause of the surface-brightness distribution. A general lack of visible dust lanes or sharp changes in surface brightness between the edges of the galaxies and the tidal features or peculiar red features in the spatial color maps supports the optically thin assumption (see Arp 232 in Fig. 5 as a counterexample and discussion of colors below). The measurements of the intensity profiles combined with the dynamical models may give us an idea of the intrinsic shape, viewing angle, and evolutionary stage of tidal features.

Average surface brightness $\bar{\mu}$ is displayed for each type of tidal feature in Fig. 10. The mean value for all features of 24.4 V mag arcsec^{-2} should *not* be taken as a true mean surface densities for tidal phenomenon since the sample is not complete in surface brightness. There do exist extremely low-surface-brightness tidal features (Malin and Carter 1983; Schombert and Bothun 1987) and this study makes no claim as to the character of tidal features as a function of surface brightness. Mean values of average surface brightness, peak surface brightness, and the dispersions are listed in Table III for comparison within the sample. Most features were remarkably constant in surface brightness having little or no gradients along long axis and sharp falloffs at the edges. This is very unlike the typical profile of a galaxy that is usually power law (e.g., $r^{1/4}$) or exponential in shape. The near constant surface brightness of the tidal features probably results from the mixing of the material from different initial radii due to the tidal interaction. Material located inside the disk can be displaced to the tidal features from a wide variety of different initial radii and azimuthal positions for disk galaxies (TT; Wallin 1989). Envelopes were the exception to this rule, usually having high average surface brightnesses and strong gradients in intensity implying that they are, to first order, spherical distributions around the primary galaxies rather than a linear or flat feature in the plane of the sky. The mean surface brightnesses of 24.4 V mag arcsec^{-1} corresponds to $7L_{\odot}$ per pc^2.

Interestingly, a large fraction of the total luminosity of these systems is found in tidal features. The mean ratio of light (and, assumably, mass) in features to light in primaries was 25%, ranging from only 3% for Arp 319 to over 60% for the envelope objects. The largest fractions were found in en-

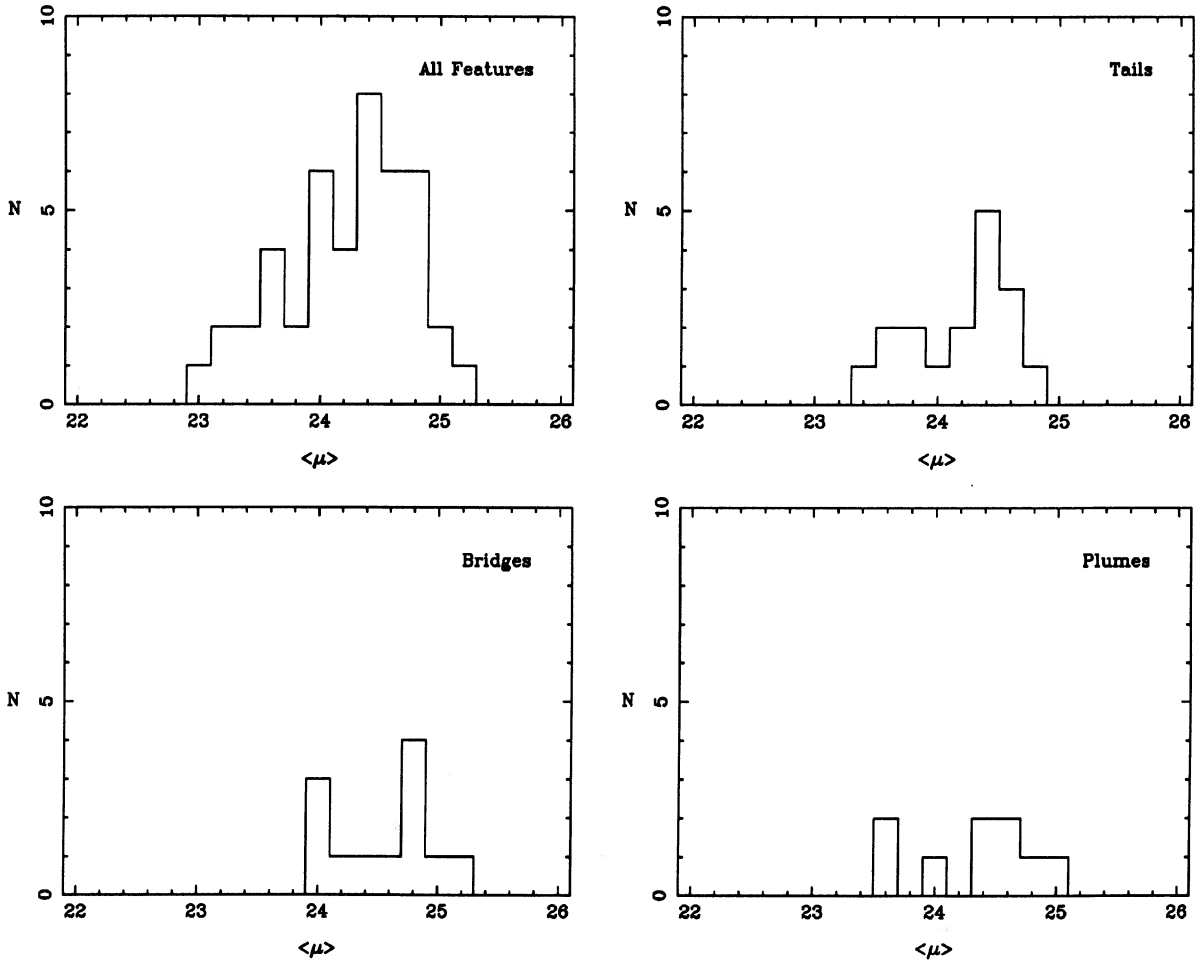

FIG. 10. Average surface brightness $\bar{\mu}$ is displayed for each type of tidal feature. The mean value for all features of 24.4 V mag arcsec^{-2} should *not* be taken as a true mean surface densities for tidal phenomenon since the sample is not complete in surface brightness. Mean values of average surface brightness, peak surface brightness, and the dispersions are listed in Table III for comparison within the sample.

TABLE III. Surface-brightness parameters.

Object	$\bar{\mu}$	μ_c
Primary	22.02±0.68	19.33±0.66
All Features	24.23±0.53	22.76±0.85
Tails	24.20±0.41	22.72±0.53
Bridges	24.56±0.40	23.11±1.13
Plumes	24.33±0.43	22.92±0.54
Envelopes	23.35±0.33	21.71±0.62

velopes, the smallest in bridges. In comparison, the shells or ripples in Arp 227 (Schombert and Wallin 1987) contained only 5% the light of the system. This material, now released from the galaxy potential, is free to distribute itself along the galaxy's orbit. If this orbit is in the core of a rich cluster, then stripped material may be the primary component of the Mpc-sized envelopes associated with first-ranked cluster members or cD galaxies. This would imply blue envelopes for cD galaxies (see mean colors for tidal features below) which are not seen (Schombert 1988). Bothun and Schombert (1989) show evidence that the main source of intracluster light is in the stripping of ellipticals bound to the cD galaxy and the type of interaction which produces the distinct tidal features are the slow, close encounters which would be rare in cluster cores, more common in the field where most of this sample is located.

In general, the intensity distribution within tidal features was smooth, missing the H II or clumpy star-forming regions common in spiral disks. However, there are several interesting exceptions to this rule (e.g., Arp 105 and Arp 245, see below) which are quite lumpy and blue. The appearance of these systems suggests that either a strong encounter has displaced an enormous percentage of disk material (gas, stars, and dust), including the active star-formation sites or that new star formation been triggered in these areas *in situ*. It is still rare in this sample to find regions within tidal features with higher surface brightness (and, therefore, stellar densities) than the primary galaxies.

b) Colors and Star Formation

The mean colors for each system component in the four bandpasses used are summarized in Table IV. Color histograms and two-color plots for each type of tidal feature are shown in Figs. 11 and 12. Note that the errors quoted in Table IV are dispersions from the mean, not errors in the measurements. Some of this dispersion is due to the contribution of Poisson noise in the measurements, particularly for the low S/N tidal features. However, most of this dispersion is spatially coherent, particularly blue regions, and is reflecting information about the history of the stellar populations (see below). Large dispersions for the primary galaxies are usually an indicator of gradients or bulge-to-disk differences. Although the present sample consists of a relatively small number of galaxies, there is great diversity among them, and an abundance of color data is provided by the CCD frames. These color data are resolved over more than two orders of magnitude in luminosity and structure size (from knots to the scale of the whole system) in some pairs. Thus, the sample potentially contains considerable information on the modes and mechanisms of star formation in galaxies, although near-infrared and optical colors do not provide a direct quantitative measure of star formation. Moreover, the problem of how best to organize this information is a formidable one. We will follow the example of LT, and many others since, in using two-color diagrams with direct comparison to normal galaxy colors and indirect comparison to color evolution calculations as our primary tools. In most cases discussed below we have preferred the $B-V$ versus $V-i$ diagram, since it has the broadest spectral coverage and the fact that the r filter could be contaminated with Hα emission.

TABLE IV. Color summary.

Object	$B-V$	$V-r$	$r-i$	$B-i$	N
Primary	0.78±0.19	0.16±0.06	0.43±0.20	1.37±0.21	48
All Features	0.64±0.24	0.11±0.11	0.44±0.23	1.19±0.26	44
Tails	0.53±0.13	0.08±0.06	0.38±0.17	0.99±0.17	17
Bridges	0.65±0.21	0.15±0.11	0.49±0.21	1.29±0.22	12
Plumes	0.66±0.31	0.08±0.17	0.40±0.26	1.14±0.27	9
Envelopes	0.93±0.07	0.18±0.04	0.58±0.27	1.69±0.25	5

1) Primary galaxies

Once we have organized the data efficiently, there still remain problems of interpretation. Perhaps the most difficult of these is the relation between colors and star-formation rates. LT were also among the first to point out that, while blue colors indicate a young stellar population, red colors do not necessarily imply the absence of such a population. They suspected that both reddening and the contribution of red supergiants could make a young population red, at least for a time. The discovery of infrared starburst galaxies in *IRAS* data (Soifer *et al.* 1987), which implies that a starburst could be almost completely buried in dust, has added a new dimension to this problem.

The color histograms in Fig. 11 and the $B-V$, $V-i$ plot in the upper left of Fig. 12 display, graphically, a summary of the mean colors of the primary galaxies in this interacting sample. A full range of galaxy types, as represented by mean colors, is seen in the sample, excluding only the very bluest systems ($B-V<0.3$). These would be the extreme dwarfs or Irr galaxies which one would expect to be easily disrupted by tidal events and, thus, would not be recognizable as an interacting pair for inclusion in the Arp Atlas. The reddest objects are elliptical-like in their contours; however, a smooth contour does not imply red color. For example, Arp 222 is much bluer than its elliptical or S0 shape would imply.

Inspection of the spatial color maps resolves a great deal of the ambiguity that the integrated colors presented. Color structure is clearly evident in many of the systems, not only as global changes such as color gradients, but as clear, distinct regions of star formation within the primary galaxies. Overall, we confirm the results from Hα imaging projects (Keel *et al.* 1985; Bushouse 1986) that a majority of the star-forming activity is confined to the cores or in rings within the primaries. However, several interesting examples of non-nuclear and tidal star formation are discussed below.

Also of interest are the color maps of the apparent merger objects (e.g. Arp 222 and 232 in Figs. 4 and 5) which show correlation between high contrast features within the galaxy

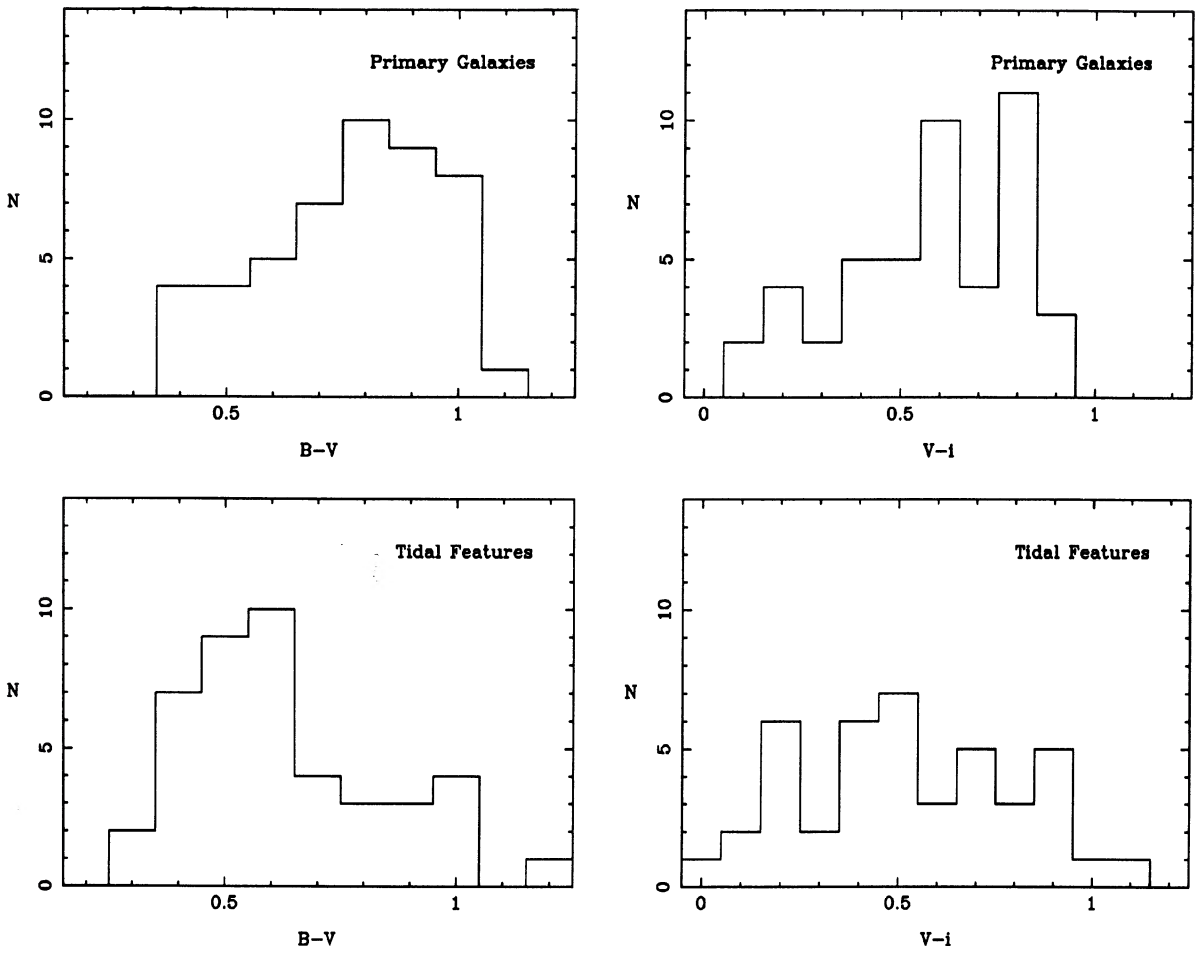

FIG. 11. Color histograms display, graphically, a summary of the mean colors of the primary galaxies and tidal features in this interacting sample. A full range of galaxy types, as represented by mean color, is seen in the sample, excluding only the very bluest systems (i.e., dwarfs, $B - V < 0.3$). The most immediate result is that the colors of tidal features are, in general, bluer than the mean colors of the primary galaxies. This value ($B - V = 0.64$) is not the extreme color normally associated with ongoing star formation (i.e., only a late-F star type population); however, neither is it typical of an old disk or halo population expected at the radii tidal features have from the center of galaxies. The bluer $B - V$ colors versus similar $V - i$ colors as compared to normal galaxies may suggest that spiral disk colors are strongly reddening and optically thick whereas tidal features are thinner and less reddened as proposed by Disney, Davies, and Phillipps (1989).

envelope and blue color. One possible interpretation is the recent cannibalism of a blue disk galaxy whose stars are now "phase-wrapped" into loops and shells within the primary galaxy's potential. This type of wrapping is predicted by the models of Quinn (1984) and Hernquist and Quinn (1989); and the blue colors are a good confirmation of the spiral or "cold" disk origin of sharp features.

For interpretation of the two-color diagram, two tracks are shown in Fig. 12: the solid line represents the colors of normal disk systems from Bothun *et al.* (1985) and the dashed line represents an infinite burst model from Wallin (1989). The data from Bothun *et al.* (1985) are aperture *UBVR* colors for several hundred spirals in ten nearby clusters. The curve in Fig. 12 represents the relationship for *disk* colors only, meaning that the bulges have been removed by subtracting inner apertures when available. The $V - R$ colors of Bothun *et al.* are converted to $V - i$ colors using a transformation designed from a program of CCD photometry of normal and low-surface-brightness spirals to be published at a later date. Although a crude measure of the stellar populations, the curve ranges from late-type Sd spirals at $B - V = 0.40$ to early-type Sa/S0 spirals with $B - V = 0.95$. The dispersion for each Hubble type is fairly constant along the curve with a mean of 0.15 mag in $B - V$. The redward turn at $V - i = 0.5$ is reflecting the increased contribution of reddening from dust in Sa to Sb types which is stronger in $B - V$ than $V - i$.

The burst model in Fig. 12 is from Wallin (1989) and the photometric code is described in full therein. Briefly, this model is similar to those produced by LT and Struck-Marcell and Tinsley (1978). The track shown is one for a burst of infinite strength, i.e., on in which all the gas is converted into stars in one massive episode of star formation. Time varies from 0 to 10 Gyr along this curve where the end product of the burst, a present day elliptical, is represented by the asterisk at the end of the track. This endpoint is redder than any object in our sample, particularly with respect to the $V - i$ color, since there are, by selection, no single age objects in

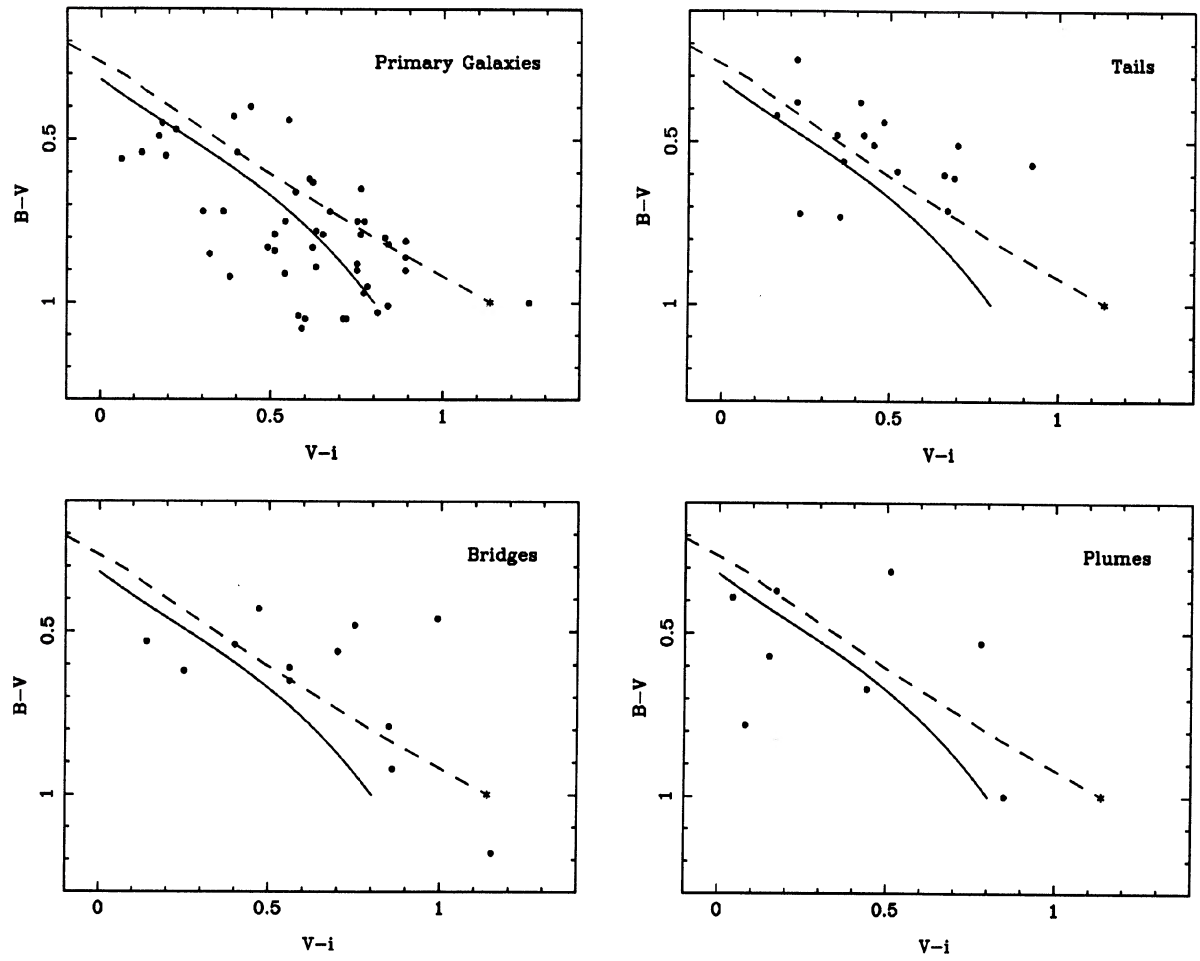

FIG. 12. Two-color diagram for the primary galaxies and tidal features, divided into plots based on overall morphology (envelopes are not shown). The distribution of the primary (brightest) galaxies does not differ from that of the secondary galaxies and the bluest colors are associated with the narrower features, meaning that tails and bridges are bluer than plumes and envelopes. Envelopes, which were only found around interacting ellipticals, are the reddest features, always as red or redder than the primary galaxies. Solid line is the track of spiral disk colors from Bothun *et al.* (1985). Dashed line is an infinite burst model from Wallin (1989). Blue regions in tidal features lie in the region defined by short bursts (10^7 yr) of low strength (1%–2%). The bluest knots in tidal features correspond to short, low mass bursts (see the text).

our sample and, in part, due to the sensitivity from extreme red giants in the synthetic colors whereas the CCD response curve diminishes the contribution from this population to the real data.

In general, the $B - V$, $V - i$ diagram confirms the results of LT that the most dramatic change in the colors of interacting galaxies is not in a shift to blue star-forming colors, but rather an increased scatter in the two-color diagram reflecting both increases and decreases in the SFR occur from tidal interactions. The scatter for the primary galaxies is 0.4 mag in $B - V$ or 3 times larger than the normal galaxy distribution. This scatter can best be explained by burst of star formation of various strengths and duration. Shorter bursts or bursts with less of the total mass converted to stars would form tracks downward from the infinite burst model at various colors. Tracks of constant star formation would form lines slightly below the relation for normal galaxies. Reddening and the color of the underlying population also serve as important parameters to any model fit to these objects (see Tinsley 1980 for a complete review of these effects).

There is a great deal of information in the spatial color maps of the main bodies concerning the location of the sites of star formation and the color–surface-brightness relation; however, this study is primarily interested in the answer to two questions. One concerns the matching of the colors of tidal features to colors in the galaxies or can a tidal feature be attributed to one or the other pair in an interaction simply by its mean color? The second question is—are there any structurally coherent features of star formation which can be linked to tidal features and, thus, to tidally induced processes? Both of these questions are addressed in the next section.

2) Tidal features

Inspection of Table IV and Fig. 11 shows that the most immediate result is that the colors of tidal features are, in general, bluer than the mean colors of the primary galaxies. This mean value ($B - V = 0.64$) is not the extreme color normally associated with ongoing star formation (i.e., only a

late-F star type population); however, neither is it typical of an old disk or halo population expected at the radii tidal features have from the center of galaxies. More enlightening is the two-color diagram for the tidal features shown in Fig. 12 divided into plots based on overall morphology (envelopes are not shown). This morphological division reveals a few weak trends. Second, the bluest colors are associated with the narrower features, meaning that tails and bridges are bluer than plumes and envelopes. Envelopes, which were only found around interacting ellipticals, are the reddest features, always as red or redder than the primary galaxies. Last, we note that the color difference between primary galaxies or normal galaxies and tidal features is almost completely due to $B - V$ differences. The $V - i$ color distribution is similar regardless of type. This leads us to believe that the primary difference is the rate of current star formation; whereas, the $V - i$ colors indicate similar old populations for both galaxies and the tidal features (i.e., an origin from common stellar material). The colors of tidal features also conforms more closely the infinite burst model than the primary or normal galaxies, again suggesting an increased rate of current star formation (see below).

Alternately, we cannot distinguish between a general enhancement of star formation in tidal features or simply a reddening difference between normal galaxies and tidal features. The same trends in Fig. 12 can be explained if spiral disks are optically thick and highly reddened, whereas tidal features are optically thin and little effected by reddening. Reddening would be dominant in the $B - V$ colors versus the $V - i$ colors and there is some suggestion of this effect in the downward curve of the normal galaxies colors for Sa types. If reddening is an important component to the integrated colors of the primary and normal galaxies than Fig. 12 would support the recent claims by Disney, Davies, and Phillipps (1989) that the low optical depths traditionally assigned to spirals is incorrect. However, the colors of tidal features, which we deduce to be optically thin, are now more directly comparable to synthetic colors from models (see below).

From dynamical models, it is clear that since the kinematic timescales for producing the tidal features are of order 10^8 yr, the presence of very blue colors in any component indicate *in situ* star formation, since the blue star lifetimes are less than the dynamical times (LT). In fact, since blue colors are not rare in these systems, we conclude that, while differential reddening may complicate the interpretation of the colors, it is probably not the dominant effect that it may be in the primary galaxies. We also note that if tidal material originates in a rich star-forming region where star formation is abruptly stopped during the tidal stripping process, then we would expect $B - V$ colors of 0.4–0.6 in only a few times 10^8 yr, and any global or local colors bluer than this are are strong indicator of ongoing star formation within the tidal feature *during* the tidal event. Comparison to LT models suggest that the blue regions in features, such as Arp 102 C, are from short, weak bursts of 10^7 yr in duration and only 1%–2% total mass in strength since they are primarily blue in $B - V$ with normal or red $V - i$ colors (i.e., occupying the upper right section of Fig. 18 from Tinsley 1980). The strongest bursts (10^8 yr and 10% total mass strength) are, of course, associated with the primary galaxies themselves where, assumably, more molecular material is available for star formation.

In addition to comparing the color distributions of the different morphologies, it is also of interest to compare the component-to-component color variations within individual systems. This is done for systems without bridges in Fig. 13, and with bridges in Fig. 14. Additionally, we have connected the component points listed in Table II within each system by line segments with no more than two segments meeting at each node, in such a way that the resulting path length in the two-color plane is minimized. Since the range of variation is roughly the same in the two colors, they are weighted equally in computing this quantity. Thus, these connected segments are essentially minimal spanning trees. If we divide the total path length in each system by the number of line segments, we get a quantity measuring the mean component-to-component color variation within the system, which we call $\langle s \rangle$. The systems with bridges tend to have somewhat larger values of $\langle s \rangle$ than, e.g., the merger remnants, which have the most homogeneous colors of all the different types of system (see Fig. 15). The inclusion of the mergers does, however, show the sensitivity of $\langle s \rangle$ as an indicator of color variations.

The quantity $\langle s \rangle$ does not seem to be very sensitive to the presence of an elliptical in the system. The bridge and tail systems containing ellipticals have $\langle s \rangle$ values distributed about equally above and below the mean. More generally, it is apparent in Figs. 13 and 14 that the path length is rarely dominated by a single long segment connecting any two component points. The difference between the average $\langle s \rangle$ values of bridge systems and mergers disappears if we divide $\langle s \rangle$ by another factor of the number of segments. This constancy of $\langle s \rangle / N$ implies that the color variations in a typical system decrease with time, as the number of components decreases (i.e., as the tidal features disappear). This is understandable if the star formation in each component is at least partially independent or uncorrelated with that in the other components. This lack of correlation is opposite to the "Holmberg" effect (Madore 1986) where the colors of interacting galaxies are correlated. The interpretation presented here is that the strength of the interaction tends to correlate the burst of star formation in the primary galaxies, but the star formation in the tidal features is from small, uncorrelated bursts of a nature very different from the large scale bursts of the primary galaxies (see below).

On the other hand, the color maps for Arp 245 and 295 show that differential reddening also likely contributes to the component-to-component color dispersion. These systems each have one nearly face-on and one nearly edge-on disk galaxy. In both systems the color difference between the two is substantial. In Arp 295 the tail of the edge-on galaxy is much bluer than its presumably reddened disk. Nonetheless, the sample does contain apparently face-on systems with large color dispersions, and other evidence for enhanced star formation.

What is the nature of the episodic star formation in individual morphological components? More than likely, there are a variety of modes and driving processes. It will suffice for the present purposes to divide these into two broad classes. The first is local, wave-driven star formation. This wave mode includes interactiondriven spiral waves in disks (Toomre 1981; Noguchi and Ishibashi 1986), spirals driven by a bar formed in the interaction (Noguchi 1987), and circular waves in ring galaxies (Lynds and Toomre 1976; Appleton and Struck-Marcell 1987; Struck-Marcell and Appleton 1987). Waves can form and propagate on different timescales in the individual galaxies and tidal features, so

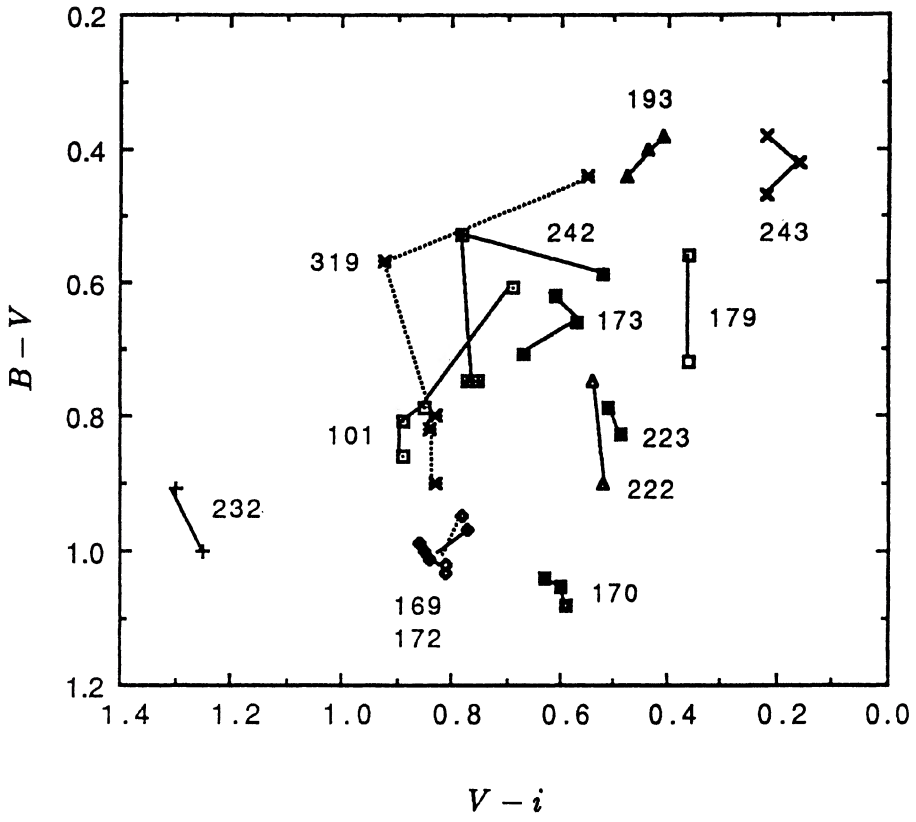

FIG. 13. Two-color diagram of individual morphological components, with all components in each system connected by straight line segments. These connections have been chosen such that the sum of the segment lengths in each system $\langle s \rangle$ is minimized (see the text).

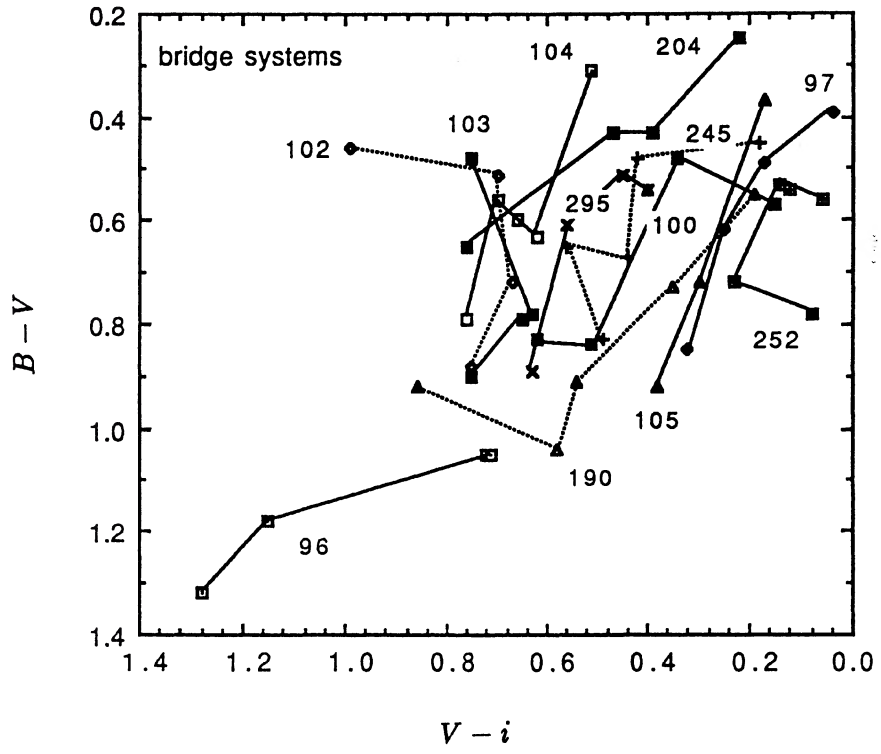

FIG. 14. Same as Fig. 13 for bridge systems only.

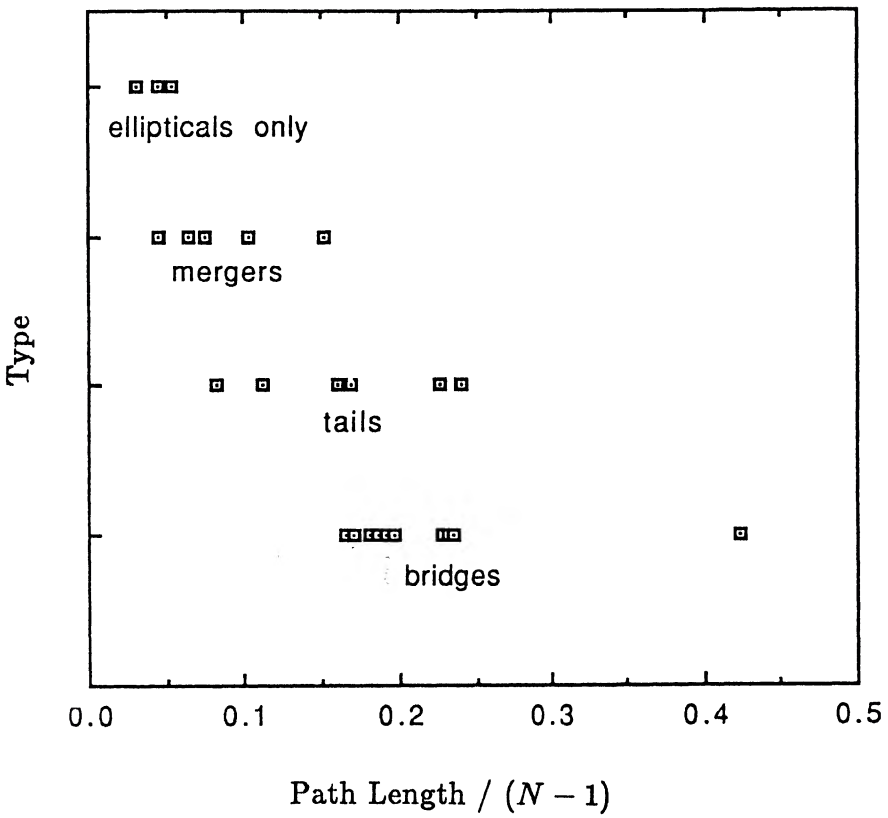

FIG. 15. System path lengths $\langle s \rangle$ from Fig. 13 divided by $N - 1$, where N is the number of morphological components for each system as listed in Table II, are plotted against system type. Bridges includes all systems with a bridge connecting two galaxies. Tails include all systems containing a tidal tail, but not a bridge. Mergers are apparent merger remnants. Ellipticals are unmerged E + E systems only. By definition, $\langle s \rangle$ increases as component-to-component color variation increases.

that the color changes resulting from wave-induced star formation can appear essentially independent in each component. Moreover, since wave compressions are usually followed by rarefaction in which star formation may be suppressed, the net SFR in a given component may not be greatly changed by the presence of a wave (see Struck-Marcell and Appleton 1987). Thus, wave-induced star formation may not have a straightforward effect on component colors.

The second mode is a global burst mode in which a large fraction of a whole component experiences a short, enhanced SFR. In this mode, the net colors of the component evolve in a similar fashion to the burst models of (LT). In general, it probably requires a violent disturbance (one with short timescales and large shock effects) to achieve the coherence across a major morphological component needed to produce a global burst. Examples might include the direct face-on collision between two gas-rich disks (Harwit *et al.* 1987), relatively rapid accretion onto a disk (Vazquez and Scalo 1989), or a very strong nuclear starburst after a large fraction of the gas has been funneled into the central regions.

In the wave mode, color dispersion across the system is expected as a result of wave-driven star formation occurring with different amplitudes and timescales in each component. In the global burst mode, color dispersion can result because different components burst at different times. However, it seems likely that in most cases, a strong burst will only occur in the primary galaxies, and not the tidal components. Then, we might expect one galaxy to dominate the color dispersion and have a high *IRAS* luminosity. Yet another possibility is that star formation might be suppressed in some components as a result of large-scale rarefaction or disruption. However, probably as a result of a selection bias against low surface brightness systems, there is little evidence for this in the present sample (but note component A of Arp 105).

Dynamical models show that most tidal features are relatively transient, with the bridges being the shortest lived. Tails form on a comparable timescale, but can persist even after the merger is accomplished (Barnes 1988). Thus, the systematic differences (e.g., in $\langle s \rangle$) between the bridge systems and the merger remnants may be the result of an age effect with a timescale comparable to the dynamical times. The fact that the values of the normalized path length $\langle s \rangle$ for tailed systems range between those of the bridges and mergers is in accord with this inference. The similar colors of bridges and tails does not contradict it (the colors of the five merger remnants are quite exceptional, even for the present sample.) If the nature of the star formation is the burst mode in the various morphological components, then these bursts may become less strong or less frequent on a dynamical timescale, for example, as a result of gas consumption or dispersion. If the star formation in each component is due to the wave mode, then we might expect the color dispersion to be large shortly after the encounter, as waves build successively in various components, and to decrease with time as waves disperse. In some systems with large color variations the

tidal components are considerably bluer than the galaxies (e.g., Arp 100, 204), but the opposite is true in others (e.g., Arp 190).

c) Dust and Gas in Tidal Features

A number of these systems were detected by *IRAS* (see Table V). The brightest of these are the merger remnants, as are the brightest extragalactic *IRAS* sources in general (Sanders *et al.* 1988). A variety of evidence suggests the presence of powerful nuclear starbursts in these strong *IRAS* sources (e.g., Soifer *et al.* 1987). Most of the nonmerged *IRAS* sources in our sample are bridge systems (plus a couple of tails). The *IRAS* detection of these dynamically young systems is certainly consistent with a significant amount of obscured star formation, though it is not possible to resolve which component or galaxy is the source of this emission.

If tidal material originated in disks of gas-rich spirals than we would expect to find similar ratios of gas-to-light and dust-to-light. H I has been detected in tidal plumes on numerous occasions; however, dust has only been detected in far-infrared emission in the Leo tidal plume (Hughes *et al.* 1989). The detection of far-infrared emission from tidal features is severely limited by the resolution and sensitivity of *IRAS*. Since the resolution of the *IRAS* satellite is comparable at 100 μm to the size of most of the tidal features, and the surface brightness expected from the tidal features low, infrared measurements of the dust-to-gas ratio may have to wait until the next generation of infrared satellites for most systems. In addition, the interstellar radiation field may be much weaker in tidal features than in disks as is implied by the lower optical surface brightnesses. However, the existence of star-forming regions in some tidal features may compensate for the low level of optical emission with additional UV flux (Bothun, Lonsdale, and Rice 1989). Similarly, the general lack of absorption dust lanes in tidal features may be the result of a lack of background light to provide contrast as in disks. When the mean surface brightness of the tidal feature is high (e.g., Arp 245), dust lanes are evident.

Two processes seem likely to produce apparent differences in the dust-to-gas ratio between disks and tidal features: starbursts in partially dust-obscured regions, and differential reddening resulting from the dynamical disturbance. The latter process might include "dereddening," for example, as a result of tidal shear and stretching reducing the dust density surrounding young star clusters or any cirrus which lies above and below the disk before the encounter. Alternately, a reduction of the dust-to-gas ratio might be expected in a low-density environment with reduced grain formation rates, but where shock and photodestruction rates might not be comparably decreased.

TABLE V. *IRAS* measurements.

Object	$f_{60\mu m}$ (Jy)	$f_{100\mu m}$ (Jy)	log f_{IR} (W m^{-2}	V (km sec^{-1})	log f_{ir} ($L_\odot$)
Arp 96	0.86	1.38	−13.34	–	–
Arp 102	0.20	1.40	−13.60	7493	9.65
Arp 104	4.07	12.25	−12.25	2884	9.88
Arp 105	4.23	6.47	−12.65	8687	10.73
Arp 173	3.67	6.48	−12.69	8725	10.69
Arp 193	14.87	23.68	−12.10	6993	11.09
Arp 204	1.84	3.42	−12.98	–	–
Arp 242	2.56	4.62	−12.84	6608	10.30
Arp 243	24.06	27.53	−11.94	5453	11.03
Arp 245N	6.76	13.98	−12.40	2313	9.83
Arp 245S	10.04	15.02	−12.28	2313	9.95
Arp 295	1.80	6.70	−12.85	6918	10.33

d) Spatial Variation of Color

We find that often the colors of tidal features matched the colors of the outer regions of disk systems. The fact that the mean color of tidal features in Table IV are bluer than the mean primary galaxy colors reflects the fact that the primary galaxy colors are averages of bulge or dusty regions and disk colors weighted by surface brightness. Therefore, the total integrated color of the primary galaxies are, in general, redder than the outer edges where one expects the tidally stripped material to originate. A excellent example of this effect is seen in Arp 190. Although the total $B - V$ color for the northern galaxy (galaxy A in Table II) is 0.72, there is a strong gradient and the outer colors match the tidal tail's $B - V$ color of 0.5. Similar effects are shown in Figs. 3 and 6 for Arp 190 and 295. In cases of an elliptical–spiral interaction, the tidal feature is blue and matches the disk colors of the spiral. As example of this is Arp 97 and 101. Both tails and bridges match the colors of the spiral and not the elliptical supporting the dynamical interpretation that thin tidal features originate from disks.

On the other hand, examples do exist in this sample of tidal features which are very blue with values indicative of vigorous current star formation. As noted above, the luminosity distribution in tidal features is usually smooth with little evidence of discrete regions of star formation. Four notable exceptions to this rule are the Arp 102 C, Arp 105 C, Arp 193 C, and Arp 245 E features. These features all have blue colors ($B - V = 0.3$–0.4) and a distinct unevenness to their surface brightness. They are not the highest-surface-brightness features in the sample, but they are above the mean. For example, Fig. 2 displays the $B - V$ color map of Arp 105. The tidal feature to the north is very blue ($B - V = 0.37$)and has several high-surface-brightness lumps that could be interpreted as H II regions. Either a large section of the disk of galaxy B has been removed intact or a low-surface-brightness late-type third galaxy is involved in the interaction.

The relatively good resolution of the CCD observations, even after averaging over several adjacent pixels, allows us to study color variations within morphological components as well as average component colors. We will not examine this data in great detail in the present paper. However, it is worthwhile to look for any systematic trends in the overall color variations within morphological components, and Fig. 16 summarizes our findings. It shows $B - V$ color dispersion σ_{B-V} in each sample component as a function of the mean $B - V$ color of the component. It appears that at each color the dispersion σ_{B-V} within tidal morphologies is greater than that of the parent galaxies. The galaxies lie within a roughly triangular locus, with the largest values of σ_{B-V} occurring when $B - V = 0.7$–0.9. It seems natural that galaxies with very red or very blue colors global colors would not also have very large internal color variations.

The relatively high values of σ_{B-V} in the tidal features could result from reddening variations as well as star-formation variations, or even to photometric errors. The tidal fea-

tures generally have very low average surface brightness, and the errors in small-scale colors are correspondingly larger. However, there are a couple of indications that photometric errors do not dominate in Fig. 16. First, (excepting a group of about eight galaxies), the dispersions σ_{B-V} and σ_{r-i} of the individual morphologies all follow a single relation with moderate scatter. If the values of σ_{B-V} and σ_{r-i} were dominated by random instrumental noise in low-surface-brightness features we would not expect this correlation. Second, even features with low mean surface brightness often have a "core" region of considerably higher surface brightness. On the other hand, the features with the highest values of σ_{B-V} have the lowest mean surface brightness.

Nonetheless, it seems unlikely that all of the separation between tidal features and galaxies in Fig. 16 is the result of photometric error. The near constancy of σ_{B-V} regardless of color, for most galaxies, seems to imply that differential reddening, rather than an enhanced star-formation rate is primarily responsible for the dispersion. In contrast, the tidal features tend to be blue, as well as having higher values of σ_{B-V} (and a larger range in those values) than the galaxies. This may well result from enhanced star formation.

Finally, we note that there is a weak correlation between σ_{B-V} and the normalized path length $\langle s \rangle$, indicating that the mean color variations on the smallest scales resolved here are comparable to those from component-to-component. This is consistent with the idea that star formation on small scales is sufficiently well organized to be responsible for large-scale color variations within the systems.

V. SUMMARY

This study presents four color optical photometry of classic interacting systems from the Arp Atlas. Our primary purpose was the investigation of the structure and stellar populations of tidal features through cross-sectional analysis and two-color grid photometry. These resulted in global luminosities and colors as well as spatial resolution to determine color variations across features. The observations and interpretation presented in this study are summarized as the following:

(1) The occurrence of tidal tails and bridges were most common in interactions between two spirals or a spiral and an elliptical. In cases where the interaction was a S + E type, the tidal feature's colors were generally the same as the disk of the spiral. Tails were more common in S + S systems, bridges more common in S + E systems. This provides new confirmation of the TT predictions that rotating disks are more susceptible to tidal features.

(2) Intensity cross sections and surface brightness suggests that plumes are face-on or near face-on sheets, and tails and bridges are more nearly one-dimensional, linear figures. Envelopes appear as radially symmetric systems surrounding the primaries.

(3) The range in colors in the primary galaxies is similar to that of normal galaxy samples. We confirm the result of LT that the difference in interacting galaxy colors is not in a strong shift towards the blue, but in a marked increase in the scatter from the normal galaxy locus. Merger objects often displayed blue loop features which are possible "phase-wrapped" young disks as predicted by the models of Hernquist and Quinn (1989) and similar to the observation of blue shells in objects from the Malin and Carter catalog.

(4) Tidal features are, in general, bluer than the primaries and it was noted that the blue colors are most dramatic in $B-V$, not $V-i$ indicating that star formation, not metallicity or age, is the dominant component. But, this observation may be due mostly to the fact that the primary colors are

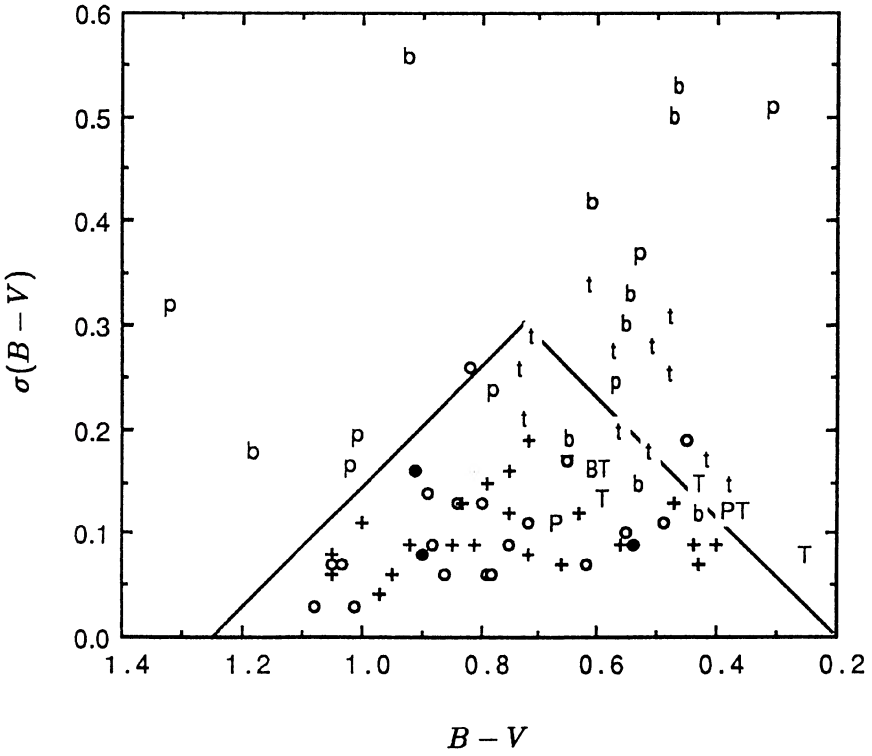

FIG. 16. Color dispersion within individual morphological components vs $B-V$ color. The symbols are defined as follows: b: bridge; t: tail; p: plume; (+): primary galaxy; circle (O); secondary galaxies. Upper case letters denote components with mean surface brightnesses of less than 24 V mag arcsec^{-2}, lower case denotes fainter components. The triangular region, which contains most of the galaxies, is drawn arbitrarily.

reddened by dust and inclusion of bulges to the integrated colors. Most of the tidal features matched the colors of the outer disks of the primary galaxies, and dispersion analysis demonstrates that a majority of the tidal debris has its origins in disks. However, some of the tidal features show areas that are both very blue and knotty in appearance indicating ongoing star formation is occurring (see Arp 105 in Fig. 2). This star formation must have occured after the material was tidally displaced from the disk since the color evolution timescale is much shorter than the dynamical timescale for the formation of tidal features. The location of these blue regions on the two-color diagram suggests they are the result of short (10^7 yr), weak (1%–2%) bursts.

(5) If tidal stripping of the nature studied here is common in clusters or groups, then the amount of luminosity made available to the intergalactic medium is large. Each encounter can liberate up to 15 to 25% of the luminosity (i.e., mass if the $\mathcal{M}/L$ of tidal features is the same as galaxies) of the interacting galaxies. This predicts that the envelopes of cD galaxies in rich cluster should be blue, as blue as an early-F type population if the halos are accreted during a collapse time of the cluster. The fact that cD envelopes are *not* blue, and are as red as the underlying elliptical (Schombert 1988) suggests either that slow interactions are rare in the cores of clusters, or that the extended features fall back into the galaxies on a relatively short timescale. Dynamical models and simple freefall timescales suggest that the latter is likely, implying that the constraints on the former process are weak.

(6) Dust and gas are present in tidal features; however, the exact ratios in most systems are unknown. Cold gas has significant concentrations in tidal features, but the limitations of *IRAS*, combined with the low level of interstellar radiation powering dust emission, make the direct detection of dust difficult (Appleton and Hughes 1988).

Given the difficulty of deconvolving the effects of reddening and star formation on colors, together with the limited size of the present sample, it is difficult to make many statistically secure statements about the nature of star formation in this sample. In particular, it is difficult to distinguish the relative importance of the different modes discussed above. The correlation between color variations on small and large scales within systems, and the fact that the large-scale variations do not generally depend on the colors of a single anomalous component, argue against the dominance of a single strong burst localized within one component. Thus, if the burst mode is responsible for the color variations, it must operate in several of the components.

Overall, the data presented here, plus the available *IRAS* data, seems consistent with the broad picture suggested in part by dynamical models of moderate star-formation enhancements driven by large-scale density waves in early encounters, followed by strong nuclear starbursts after the dominant galaxies have merged. At the same time the data do not exclude many other variations on this scenario, including global bursts throughout a disk after an especially violent encounter (as in Bushouse 1986) or global suppressions that might follow such a burst (Scalo and Struck-Marcell 1986). We should also note that, primarily because of a lack of data, we can say little about the role of different gas masses in interacting systems. Further 21 cm and CO studies are undoubtedly the key needed to unlock the connection between dynamics and star formation.

We wish to thank the referee, R. Kennicutt, for his comments which greatly improved this paper. We also thank Palomar Observatory and the mountain staff for the allocation of time and assistance at the telescopes.

REFERENCES

Appleton, P. N., and Hughes, D. H. (1988). In *Dust in the Universe*, edited by M. E. Bailey and D. A. Williams (Cambridge University, Cambridge), p. 483.
Appleton, P. N., and Struck-Marcell, C. (1987). Astrophys. J. **318**, 103.
Arp, H. C. (1966). *Atlas of Peculiar Galaxies* (California Institute of Technology, Pasadena).
Barnes, J. E. (1988). Apstrophys. J. **331**, 699.
Barsony, M. (1988). Ph.D. thesis, California Institute of Technology.
Bothun, G. D. (1986). Astron. J. **94**, 507.
Bothun, G. D., Aaronson, M., Schommer, B., Mould, J., Huchra, J. and Sullivan, W. T. (1985). Astrophys. J. Suppl. **57**, 423.
Bothun, G. D., Lonsdale, C. J., and Rice, W. (1989). Astrophys. J. **341**, 129.
Bothun, G. D., and Schombert, J. M. (1990). Astrophys. J. (in press).
Bushouse, H. A. (1986). Astrophys. J. **91**, 255.
Condon, J. J. (1983). Astrophys. J. Suppl. **53**, 459.
Disney, M., Davies, J., and Phillipps, S. (1989). Mon. Not. R. Astron. Soc. **239**, 939.
Harwit, M., Houck, J. R., Soifer, B. T., and Palumbo, G. G. C. (1987). Astrophys. J. **315**, 28.
Hernquist, L., and Quinn P. (1989). Astrophys. J. **342**, 1.
Huchra, J. P. (1977). Astrophys. J. **217**, 928.
Hughes, D. H., Appleton, P. N., and Schombert, J. M. (1989). In preparation.
Joseph, R. D., and Wright, G. S. (1985). Mon. Not. R. Astron. Soc. **214**, 87.
Keel, W. C., Kennicutt, R. C., Hummel, E., and van der Hulst, J. M. (1985). Astron. J. **90**, 708.
Kennicutt, R. C. (1989). Preprint.
Kennicutt, R. C., Heel, W. C., van der Hulst, J. M., Hummel, E., and Roettiger, K. A. (1987). Astron. J. **93**, 1011.
Kent, S. M. (1985). Publ. Astron. Soc. Pac. **97**, 165.
Landolt, A. (1983). Astron. J. **88**, 439.
Larson, R. B., and Tinsley, B. M. (1978). Astrophys. J. **219**, 46.
Lynds, R., and Toomre, A. (1976). Astrophys. J. **209**, 382.
Madore, B. F. (1986). In *Spectral Evolution of Galaxies*, edited by C. Chiosi and A. Renzini (Reidel, Boston), p. 97.
Malin, D. F., and Carter, D. (1983). Astrophys. J. **274**, 534.
Noguchi, M. (1987). Mon Not. R. Astron. Soc. **228**, 635.
Noguchi, M., and Ishibashi, S. (1986). Mon. Not. R. Astron. Soc. **219**, 305.
Quinn, P. J. (1984). Astrophys. J. **274**, 596.
Rieke, G. H., Lebofsky, M. J., Thompson, R. I., Low, F. J., and Tokunaga, A. T. (1980). Astrophys. J. **238**, 905.
Sanders, D. B., Soifer, B. T., Elias, J. H., Madore, B. F., Matthews, G., Neugebauer, G., and Scoville, N. Z. (1988). Astrophys. J. **325**, 74.
Scalo J. M., and Struck-Marcell, C. (1986). Astrophys. J. **301**, 77.
Schombert, J. M. (1988). Astrophys. J. **328**, 475.
Schombert, J. M., and Wallin, J. F. (1987). Astron. J. **94**, 300.
Schombert, J. M. and Bothun, G. D. (1987). Astron. J. **95**, 1389.
Schweizer, F. (1986). Science **231**, 227.
Schweizer, F., and Seitzer, P. (1988). Astrophys. J. **328**, 88.
Soifer, B. T., Houck, J. R., and Neugebauer, G. (1987). *Annual Review of Astronomy and Astrophysics*, edited by G. Burbridge, D. Layzer, and J. G. Phillips (Annual Reviews Inc., Palo Alto, CA), Vol. 25, p. 187.
Struck-Marcell, C., and Appleton, P. N. (1987). Astrophys. J. **323**, 480.

Struck-Marcell, C., and Tinsley, B. M. (1978). Astrophys. J. **221**, 562.
Telesco, C. M. (1984). In *Proceedings of the Workshop on Star Formation*, edited by R. D. Wolstencroft (Royal Observatory, Edinburgh), p. 183.
Telesco, C. M., Wolstencroft, R. D., and Done, C. (1988). Astrophys. J. **329**, 174.
Tinsley, B. M. (1980). Fundam. Cosmic Phys. **5**, 287.
Thronson, H. A., Hunter, D. A., Telesco, C. M., Harper, D. A., and Decher, R. (1987). Astrophys. J. **317**, 180.
Toomre, A. (1981). In *The Structure and Evolution of Normal Galaxies*, edited by S. M. Fall and D. Lynden-Bell (Cambridge University, Cambridge).
Toomre, A., and Toomre, J. (1972). Astrophys. J. **178**, 623 (TT).
Vazquez, A., and Scalo, J.M. (1989). Astrophys. J. (in press).
Vorontsov-Velyaminov, B. A. (1959). *Atlas and Catalog Interacting Galaxies* (Sternberg State Astronomical Institute, Moscow).
Wallin, J. F. (1989). Ph.D. thesis, Iowa State University.